Contrib Mineral Petrol (2013) 165:305–326
DOI 10.1007/s00410-012-0810-0

ORIGINAL PAPER

Constraints from melt inclusions and their host olivines on the petrogenesis of Oligocene-Early Miocene Xindian basalts, Chifeng area, North China Craton

L.-B. Hong · Y.-H. Zhang · S.-P. Qian · J.-Q. Liu · Z.-Y. Ren · Y.-G. Xu

Received: 11 March 2012 / Accepted: 3 September 2012 / Published online: 22 September 2012

Abstract The geochemical characteristics of melt inclusions and their host olivines provide important information on the processes that create magmas and the nature of their mantle and crustal source regions. We report chemical compositions of melt inclusions, their host olivines and bulk rocks of Xindian basalts in Chifeng area, North China Craton. Compositions of both bulk rocks and melt inclusions are tholeiitic. Based on petrographic observations and compositional variation of melt inclusions, the crystallizing sequence of Xindian basalts is as follows: olivine (at MgO > ~5.5 wt%), plagioclase (beginning at MgO = ~5.5 wt%), clinopyroxene and ilmenite (at MgO < 5.0 wt%). High Ni contents and Fe/Mn ratios, and low Ca and Mn contents in olivine phenocrysts, combining with low CaO contents of relatively high MgO melt inclusions (MgO > 6 wt%), indicate that Xindian basalts are possibly derived from a pyroxenite source rather than a peridotite source. In the CS-MS-A diagram, all the high MgO melt inclusions (MgO > 6.0 wt%) project in the field between garnet + clinopyroxene + liquid and garnet + clinopyroxene + orthopyroxene + liquid near 3.0 GPa, further suggesting that residual minerals are mainly garnet and clinopyroxene, with possible presence of orthopyroxene, but without olivine. Modeling calculations using MELTS show that the water content of Xindian basalts is 0.3–0.7 wt% at MgO = 8.13 wt%. Using 20–25 % of partial melting estimated by moderately incompatible element ratios, the water content in the source of Xindian basalts is inferred to be ≥450 ppm, much higher than 6–85 ppm in dry lithospheric mantle. The melting depth is inferred to be ~3.0 GPa, much deeper than that of tholeiitic lavas (<2.0 GPa), assuming a peridotite source with a normal mantle potential temperature. Such melting depth is virtually equal to the thickness of lithosphere beneath Chifeng area (~100 km), suggesting that Xindian basalts are derived from the asthenospheric mantle, if the lithospheric lid effect model is assumed.

Keywords Melt inclusion · Olivine chemistry · Pyroxenite source · Water · Basalts · North China Craton

Communicated by T. L. Grove.

L.-B. Hong · Y.-H. Zhang · S.-P. Qian · J.-Q. Liu · Z.-Y. Ren (✉) · Y.-G. Xu
State Key Laboratory of Isotope Geochemistry, Guangzhou Institute of Geochemistry, Chinese Academy of Sciences, Wushan, Guangzhou 510640, People's Republic of China
e-mail: zyren@gig.ac.cn

L.-B. Hong · Y.-H. Zhang · S.-P. Qian · J.-Q. Liu
University of Chinese Academy of Sciences, Beijing 100049, People's Republic of China

Introduction

For years, it was thought that peridotite (olivine mode >40 %), the predominant lithology in the upper mantle, is the source of mafic magmas (peridotite melts; e.g., Green and Ringwood 1963; Ringwood 1975; McKenzie and Bickle 1988; McDonough and Sun 1995). Based on this assumption, with a normal mantle potential temperature, the melting depth of alkali basalts is inferred to be deeper than that of tholeiitic basalts, and the alkali-to-tholeiitic transition would occur at depth of 40–60 km (e.g., DePaolo and Daley 2000). Thus, the temporal variation in lithospheric thickness can be reconstructed (DePaolo and Daley 2000; Xu et al. 2004), if three conditions are meet: (1) Basalts are confirmed to be derived from asthenospheric mantle with a normal mantle potential temperature; (2) change of volcanic mafic rock type

(e.g., from tholeiitic basalts to alkali basalts) with time is defined; and (3) the lithospheric lid effect model (the final melting depth is controlled by the thickness of lithosphere above) is assumed (e.g., Niu et al. 2011).

However, this conventional view is challenged, because melting of pyroxenite, another lithology primarily composed of pyroxene, garnet and possibly olivine (olivine mode <40 %; Kogiso et al. 2004), can also produce basalts (pyroxenite melts; e.g., Hofmann and White 1982; Weaver 1991; Hauri and Hart 1993; Hirschmann and Stolper 1996; Hauri 1996; Hofmann 1997; Lassiter and Hauri 1998; Stracke et al. 2003, 2005; Ren et al. 2004, 2005, 2006, 2009; Kogiso et al. 2004). Compared with peridotite, pyroxenite has lower solidus and shorter melting interval, corresponding to greater melting depth and higher melt productivity (e.g., Yasuda et al. 1994; Takahashi et al. 1998). This suggests that the alkali-to-tholeiitic transition could occur deeper than previously thought. It is thus pivotal to identify the source lithology of basalts before discussing their petrogenesis.

Cenozoic basalts are widespread in eastern North China Craton (NCC) (Fig. 1a). They were thought to be peridotite melts formed in asthenospheric mantle (e.g., Fan and Hooper 1991; Xu 2001). The rock types of these basalts gradually change from tholeiitic basalts with subordinate subalkali basalts in Early Tertiary to alkali and strongly

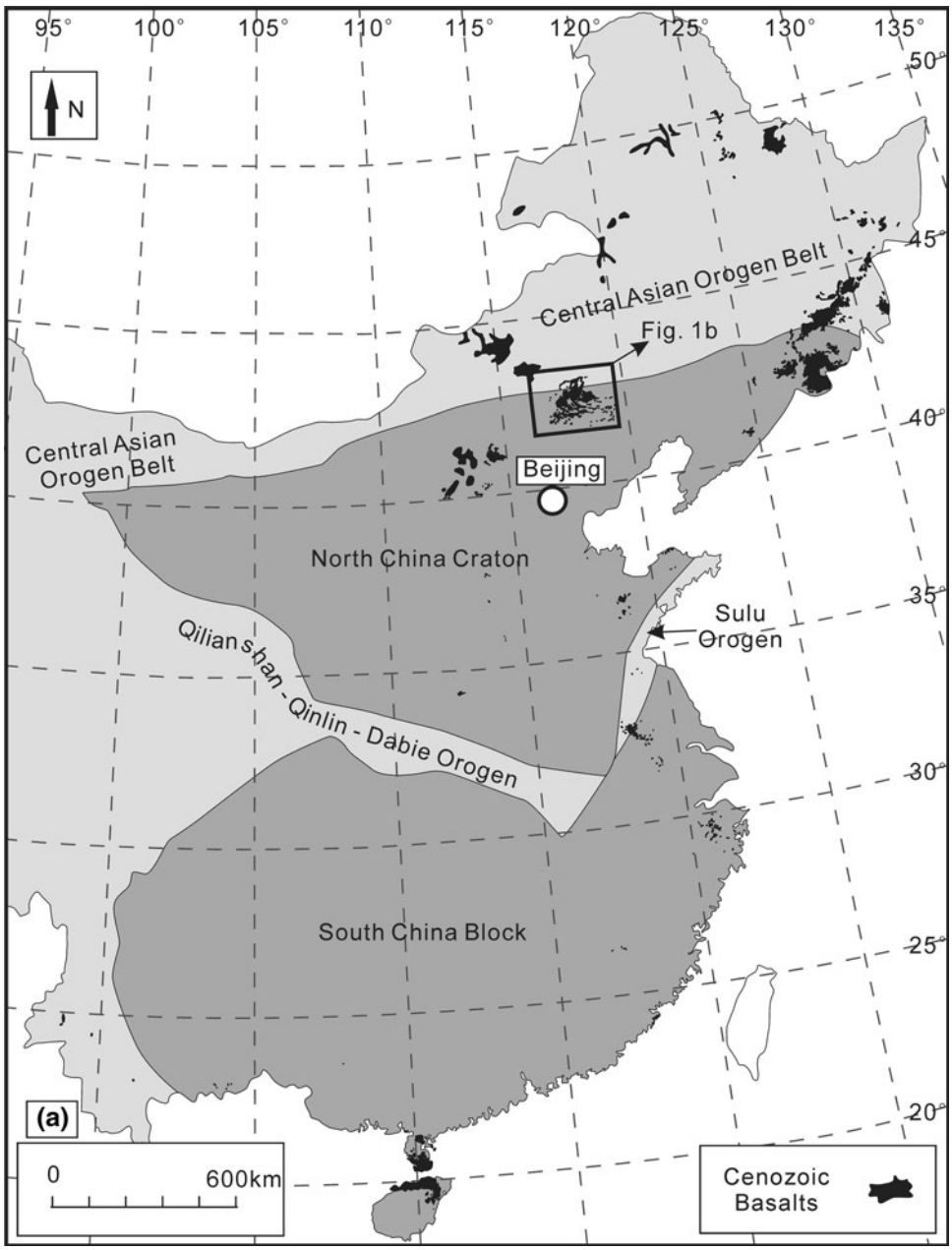

Fig. 1 **a** Simplified geological map of eastern China. **b** Distribution of Cenozoic basalts in Chifeng area, northern edge of the NCC (modified after Jia et al. 2002). The location of Xindian basalts is marked with black four-point star in the southeastern side of the area

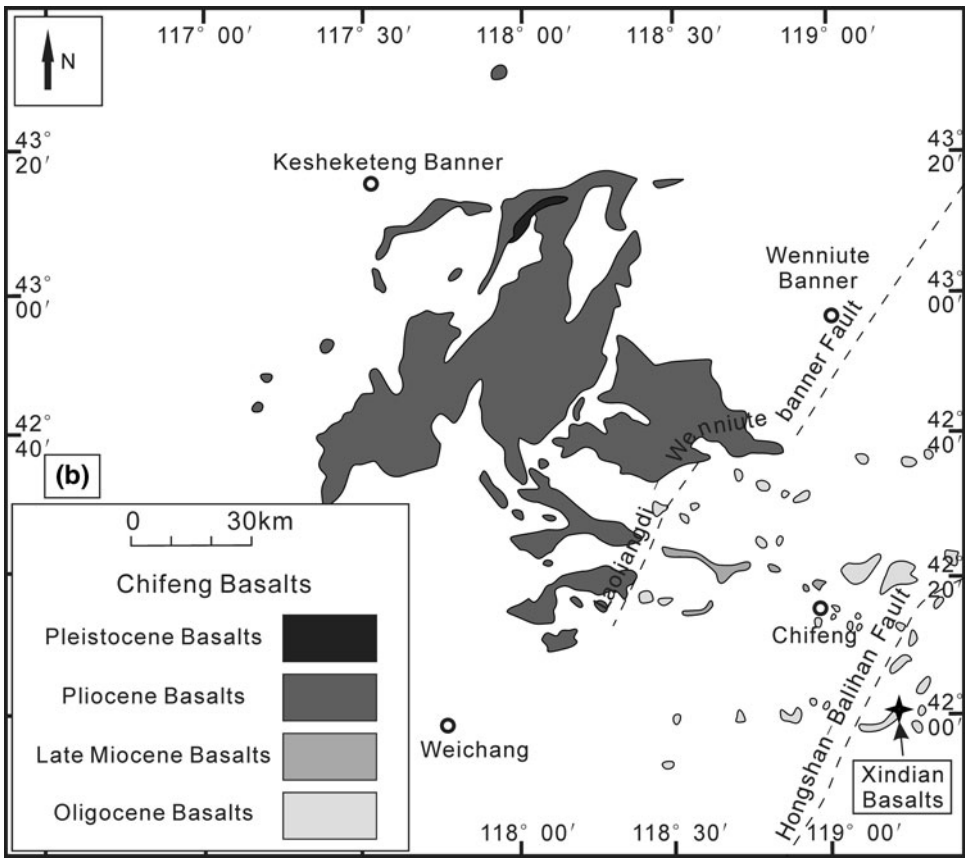

Fig. 1 continued

alkali basalts in Late Tertiary and Quaternary (Fan and Hooper 1991; Liu et al. 1992a; Menzies and Xu 1998; Xu 2001, 2007; Xu et al. 2004). In view of the normal mantle potential temperature in the eastern NCC during Cenozoic, this temporal variation of basalts was explained as a result of lithospheric thickening during Cenozoic (Menzies and Xu 1998; Xu 2001, 2007; Xu et al. 2004). However, recent studies on Cenozoic basalts from Shandong province, Subei basin and Shuangliao, eastern NCC, showed that basalts from these areas were pyroxenite melts (Chen et al. 2009; Zhang et al. 2009; Wang et al. 2011; Zeng et al. 2011; Xu et al. 2012), thus casting doubt on the previous assumption of peridotite melts and assessment on variation in lithospheric thickness. Moreover, these existing studies were mainly focused on alkali basalts, but tholeiitic basalts were paid less attention, possibly due to their limited distribution in these areas. Besides, basalts of several volcanoes in all these recent studies were investigated together, and fractional crystallization was poorly constrained in a single volcano, due to little variation of major elements of bulk rocks (e.g., Zhang et al. 2009; Zeng et al. 2011). Last but not least, H_2O is important for magma formation (e.g., Kushiro 1968, 1969, 1972; Mysen et al. 1980; Gaetani and Grove 1998; Falloon and Danyushevsky 2000; Asimow and Langmuir 2003; Asimow et al. 2004; Parman and Grove 2004; Liu et al. 2006; Wood and Turner 2009). Yet, up to now, the water contents of Cenozoic basalts in NCC have still not been constrained.

Olivine chemistry has the potential ability to identify the source lithology (e.g., Herzberg 2011; Putirka et al. 2011). Ni and Ca are compatible in olivine and clinopyroxene, respectively (Hart and Davis 1978; Kinzler et al. 1990; Beattie et al. 1991; Herzberg 2006; Herzberg and Asimow 2008), while Mn prefers to enter garnet (Pertermann and Hirschmann 2003; Balta et al. 2011). Thus, compared to peridotite melts, pyroxenite melts have higher Ni contents and Fe/Mn ratios, but lower Ca and Mn contents, due to higher garnet and clinopyroxene mode, but lower olivine mode in the residual source. Olivine, commonly crystallizing at the early stage, will inherit these features. In other words, olivines from pyroxenite melts will have higher Ni and Fe/Mn, but lower Ca and Mn (e.g., Sobolev et al. 2007; Herzberg 2011).

Melt inclusions are little magma droplets trapped in crystals during their growth within magmatic systems (Sorby 1858; Roedder 1979). They can record information on volatile contents before eruption and petrogenetic processes such as crystallization, magma mixing and crustal contamination and allow reconstruction of the primary melt compositions (Sobolev and Kostyuk 1975; Sobolev 1996;

Lowenstern 1995, 2003; Frezzotti 2001; Danyushevsky et al. 2002; Schiano 2003; Ren et al. 2005; Kamenetsky 2006; Kent 2008; Métrich and Wallace 2008; Moore 2008; Blundy and Cashman 2008; and references in these papers). Comparing with whole rocks, melt inclusions have advantages as below (Kent 2008): (1) Because of being trapped in different minerals growing at various stages of magma evolution, melt inclusions often bear wider compositions than bulk rocks (e.g., Sobolev and Shimizu 1993; Nielsen et al. 1995; Gurenko and Chaussidon 1995; Saal et al. 1998, 2005; Kent et al. 1999, 2002; Norman et al. 2002; Sours-Page et al. 2002; Ren et al. 2004, 2005; Jackson and Hart 2006; Kamenetsky and Gurenko 2007). More importantly, compositions of melt inclusions within the earliest mineral phenocrysts, for example, olivines with the highest Fo, are comparable to those of the primitive magmas (e.g., Sobolev and Shimizu 1993; Sobolev 1996). (2) Now that being trapped at relatively high pressure, melt inclusions could preserve volatile components (such as H_2O, S, Cl and CO_2) of magmas well, which could be measured directly (e.g., Sobolev and Chaussidon 1996; Kovalenko et al. 2000; Walker et al. 2003; Portnyagin et al. 2007). (3) Melt inclusions within resistant phenocrysts would survive from alteration if they remain closed all the time (e.g., McDonough and Ireland 1993).

In this study, we chose Xindian tholeiitic basalts in Chifeng area as the object, because tholeiitic basalts in this area are distributed relatively widely (Fig. 1b), and previous studies on these basalts in the area were focused on petrology, geochronology and paleointensity (Luo and Chen 1990; Liu et al. 1992c; Jia et al. 2002; Zheng et al. 2002; Shi et al. 2002, 2005; Zhao et al. 2004), but geochemical studies are in low quality. Combining chemical compositions of bulk rocks, melt inclusions and their host olivine crystals, we try to reach these aims: (1) to understand the crystal crystallization sequence and process of Xindian basalts; (2) to identify the source lithology; and (3) to estimate the H_2O content of Xindian basalts.

Geological background and petrography

The NCC is one of the oldest cratons in the world (up to 3.8 Ga; Jahn et al. 1987; Liu et al. 1992b; Song et al. 1996; Zheng et al. 2004; Wu et al. 2005a). Its western and northern boundaries are the Early Paleozoic Qilianshan Orogen and the Late Paleozoic Central Asian Orogenic Belt, respectively. In the south, Sulu-Dabie-Qiling Orogen separates the NCC from South China Block (Fig. 1a).

Since being an integrated craton, the NCC had been stable until kimberlites eruption in Early Paleozoic. Studies on peridotites captured in these kimberlites point to a thick (>180 km), cold (<40mW/m^2), old (>2.5 Ga) and refractory cratonic subcontinental lithospheric mantle (SCLM) beneath the NCC during Early Paleozoic (e.g., Menzies et al. 1993; Griffin et al. 1998; Gao et al. 2002; Chu et al. 2009). However, since Mesozoic, especially Late Mesozoic, the NCC has been destabilized, as expressed by intense magma activities (Xu et al. 2009; and references therein). The mantle xenoliths entrained by Cenozoic basalts further reveal that Cenozoic SCLM beneath eastern NCC is thin (<80 km), hot ($\sim$65mW/m^2), young and fertile (e.g., Menzies and Xu 1998; Zheng et al. 1998, 2006; Fan et al. 2000; Gao et al. 2002; Rudnick et al. 2004; Xu and Bodinier 2004; Chu et al. 2009). This suggests a removal of >100 km of Archean lithosphere during Phanerozoic (Menzies et al. 1993; Griffin et al. 1998; Fan et al. 2000).

The mechanism of the NCC destruction is strongly debated. So far, two extreme models exist: the delamination model (e.g., Wu et al. 2000, 2003; Gao et al. 2002, 2004, 2008; Chu et al. 2009) and the thermal–mechanical erosion model (e.g., Griffin et al. 1998; Menzies and Xu 1998; Xu 2001; Menzies et al. 2007). In the delamination model, the thickened eclogitic lower crust, together with the lithospheric mantle below, delaminates into the convection mantle. However, this model fails to answer two main questions. (1) The difference in density between the eclogite and cratonic SCLM is not large enough to succeed in delaminating the whole thick SCLM (e.g., Xu 2001). (2) The destruction period of NCC lasts more than 100 Ma (e.g., Xu 2001), rather than a short time interval expected by delamination (<10 Ma; e.g., Lustrino 2005). In thermal–mechanical erosion model, the upwelling hot materials below the SCLM, that is, mantle plume, bring heat to bake and soften the lowest part of SCLM, resulting in its removal gradually by the horizon shear force of asthenosphere. Meanwhile, melts, produced by decompression melting of hot materials, rise up and metasomatize the refractory SCLM into more fertility, which benefits the SCLM removal. The disadvantage of this model is the following: (1) no evidence for mantle plume existing below the NCC during the destruction period (Niu 2005); (2) magmatism focusing on two peaks, 195–150 Ma and 130–120 Ma, rather than a gradual, long-lived event (Wu et al. 2005b, c).

Chifeng area is located in the northern edge of the NCC (Fig. 1a). Accompanying the destruction of NCC and the asthenosphere upwelling, a large area of basalts has been erupted in this area since Late Cretaceous, especially during Cenozoic periods (Fig. 1b; Luo and Chen 1990; Liu et al. 1992c; Han et al. 1999; Jia et al. 2002; Zheng et al. 2002; Zhang et al. 2003; Zhao et al. 2004; Shi et al. 2005). According to Jia et al. (2002), basalts in Chifeng area could be divided into four epochs: Oligocene (mainly >20 Ma), Late Miocene (6–10 Ma), Pliocene ($\sim$5 Ma)

and Pleistocene (<1 Ma). Basalts of the former two episodes are mainly distributed between Laoliangdi–Wenniute Banner Fault and Hongshan–Balihan Fault in the southeast (Fig. 1b). Both of them are mainly tholeiitic basalts. Basalts of the latter two episodes, mainly distributed to northwest of Laoliangdi–Wenniute Banner Fault (Fig. 1b), are dominated by alkali basalts. Thus, from the southeast to the northwest, Cenozoic eruptions in Chifeng area gradually get younger. The Xindian basalts are located in the southeast of Chifeng area and were erupted in Late Oligocene to Early Miocene (22–24 Ma; Shi et al. 2002).

All the samples of Xindian basalts reported in this study are gray black color and compact massive structure. In thin sections, ~1 vol % phenocrysts (≧0.5 mm) scatter the matrix. They are mainly euhedral and subhedral olivines. Some of them are altered due to the oxidation on the surface while others still remain fresh. Melt inclusions with round to elliptic shape and filamentous microminerals can be found in some fresh olivine phenocrysts. Rarely, plagioclase phenocrysts (~0.5 mm) with the appearance of short plate are identified. All of the observed plagioclase phenocrysts show resorption pitted texture in the cores. The intergranular to subophitic texture of the matrix is composed of plagioclase and ilmenite, anhedral olivine and clinopyroxene, and glass, with the size less than 0.5 mm.

Materials and methods

Sample preparation

Samples of Xindian basalts were firstly sawn into slabs. After selecting pieces for making thin sections, all residuals were broken into chips, with the fresh ones grounded into powder for chemical analysis, and the others for olivine grain selection. All the analyses were conducted in State Key Laboratory of Isotope Geochemistry, Guangzhou Institute of Geochemistry, Chinese Academy of Sciences (GIG-CAS).

Bulk rock analysis

Major element analyses of five bulk rocks were carried out by X-ray fluorescence spectrometry (XRF) on fused glass disks using Rigaku ZSX-100e XRF instrument. Analytical procedure is described by Goto and Tatsumi (1996). The same samples were also analyzed for trace elements by Thermo Scientific XSERIES 2 inductively coupled plasma-mass spectrometry (ICP-MS), using techniques described by Liu et al. (1996). Precisions for most trace elements were better than 5 %.

Olivine and melt inclusion analysis

In view of the occurrence of post-crystallization, homogenization of melt inclusions is required. Such process was described in detail by Ren et al. (2005); 1 atm gas mixing furnace was used, and the oxygen fugacity was kept at the quartz–fayalite–magnetite (QFM) buffer. After being heated at 1,250 °C for 10 min, olivines were quickly elevated to the top of the furnace and held there for quench. Later, olivines were mounted in epoxy resin disks and polished until the glassy inclusions were exposed on the surface.

A total of 53 olivine grains and 36 melt inclusions enclosed in olivines were analyzed by electron probe microanalysis (EPMA) with a JEOL JXA-8100 Superprobe, following the procedures of Sobolev et al. (2007) for olivines and Wang and Gaetani (2008) for melt inclusions. The operating conditions are as follows: 20 kV accelerating voltage, 300 nA beam current and 2 μm beam diameter for olivine analysis, and 15 kV accelerating voltage, 20 nA beam current and 3 μm beam diameter for melt inclusion analysis. For melt inclusions, Na and K were measured first in each analysis, and 10 s for peak counting time and 5 s for background counting time on both sides were used to minimize their possible loss during analysis. To monitor machine drift, an internal olivine and an internal glass standard (JB-2) were analyzed before and after each batch analysis. The relative analytical uncertainty (relative standard deviation) for the internal olivine standard is 0.1–0.4 % for major elements (SiO_2, MgO and FeO), and 1–3 % for minor elements (CaO, MnO and NiO), and for JB-2 is <0.5 % for most major elements (5, 1 and 8 % for MnO, K_2O and P_2O_5, respectively).

Results

Compositions of bulk rocks and melt inclusions

Major element compositions of five samples studied in this paper are very similar, with MgO contents ranging from 7.2 to 7.5 wt% (Table 1). The range of MgO contents of melt inclusions in Xindian basalts before Fe-loss correction is from 7.2 to 9.8 wt%, slightly wider than those of whole rocks (Table 2). There is a negative correlation between FeO contents of melt inclusions and Fo values of host olivines, the so-called Fe-loss (Fig. 2a), which is caused by post-entrapment re-equilibration between melt inclusions and their host olivines (e.g., Danyushevsky et al. 2000). The measured major element compositions of these inclusions therefore need to be recalculated. CaO/Al_2O_3 ratios of melt inclusions are nearly constant (Fig. 2b), suggesting that these melt inclusions only experienced olivine

Table 1 Major and trace element compositions of bulk rocks of Xindian basalts analyzed by XRF and ICP-MS, respectively

Sample	XD10-1	XD10-2	XD10-3	XD10-4	XD10-5
Rock type	Tholeiitic rocks				
XRF (wt%)					
SiO_2	50.87	50.86	50.92	50.92	50.88
TiO_2	2.20	2.17	2.24	2.31	2.21
Al_2O_3	13.41	13.53	13.43	13.34	13.45
Fe_2O_3	13.21	13.10	13.29	13.34	13.25
MnO	0.15	0.15	0.15	0.15	0.15
MgO	7.46	7.49	7.40	7.22	7.42
CaO	8.43	8.50	8.47	8.37	8.44
Na_2O	2.65	2.64	2.66	2.72	2.66
K_2O	0.89	0.90	0.89	1.01	0.91
P_2O_5	0.35	0.34	0.35	0.36	0.35
L.O.I	0.07	0.01	−0.11	−0.07	−0.03
Total	99.69	99.69	99.69	99.69	99.69
XRF (ppm)					
Cr	273	257	262	261	260
Ni	161	162	155	157	160
Zr	158	154	159	164	159
Nb	19.6	20.5	19.5	20.3	18.7
ICP-MS (ppm)					
Sc	21.0	21.1	20.7	20.9	21.0
Cs	0.177	0.182	0.159	0.182	0.167
Ba	236	228	240	247	239
Rb	14.5	14.8	14.3	16.2	14.7
Sr	383	393	386	386	388
Ti	12,780	12,660	12,620	13,280	12,750
Y	24.7	24.8	24.7	25.8	24.8
Zr	156	157	161	163	158
Nb	18.1	18.3	18.5	18.8	18.3
Hf	4.04	4.11	4.12	4.17	4.01
Ta	1.22	1.13	1.21	1.24	1.17
Th	2.13	2.12	2.16	2.21	2.15
U	0.467	0.472	0.489	0.502	0.476
La	19.0	18.9	19.0	19.7	18.9
Ce	39.7	39.7	40.7	42.8	39.7
Pr	5.33	5.31	5.45	5.56	5.30
Nd	23.5	23.5	23.9	24.1	23.3
Sm	5.65	5.80	5.72	5.87	5.66
Eu	1.90	1.94	1.96	1.96	1.88
Gd	5.86	5.91	5.85	5.99	5.84
Tb	0.905	0.909	0.914	0.936	0.898
Dy	5.00	4.92	5.02	5.12	5.08
Ho	0.933	0.929	0.952	0.939	0.932
Er	2.27	2.28	2.26	2.24	2.26
Tm	0.286	0.301	0.280	0.302	0.298
Yb	1.63	1.69	1.66	1.77	1.78
Lu	0.234	0.250	0.253	0.256	0.250
La/Yb	11.7	11.2	11.4	11.1	10.6

Table 2 Major element compositions of melt inclusions of Xindian basalts analyzed by EPMA

	SiO_2	TiO_2	Al_2O_3	FeO	MnO	MgO	CaO	Na_2O	K_2O	P_2O_5	NiO	Total	Fo
XD10-(1)-1	51.77	2.26	13.59	9.76	0.11	9.22	8.05	3.33	0.94	0.35	0.03	99.42	80.76
XD10-(1)-2	48.74	1.93	11.98	17.25	0.17	8.38	7.17	2.99	0.83	0.32	0.01	99.78	76.00
XD10-(1)-6A	51.28	2.07	13.28	12.22	0.12	8.42	7.67	3.27	0.90	0.38	0.05	99.66	78.58
XD10-(1)-6B	49.54	2.11	12.72	14.95	0.16	8.37	7.98	2.65	0.77	0.35	0.05	99.64	79.41
XD10-(1)-7	50.39	2.27	13.11	13.06	0.14	8.17	8.27	3.20	0.81	0.37	0.05	99.83	80.20
XD10-(2)-1	51.64	2.32	13.83	11.02	0.12	7.74	7.92	3.54	0.91	0.43	0.03	99.50	81.54
XD10-(2)-1/B	51.16	2.13	13.51	11.44	0.12	8.51	8.23	2.92	0.82	0.38	0.03	99.26	80.04
XD10-(2)-1/C	51.49	2.14	13.68	11.13	0.12	8.13	8.33	3.18	0.80	0.47	0.02	99.50	80.90
XD10-(2)-2	49.34	2.10	12.36	12.89	0.14	7.26	7.84	3.02	0.85	0.36	0.02	96.16	80.27
XD10-(2)-3	50.05	2.17	12.89	13.55	0.15	9.11	7.48	2.89	0.93	0.35	0.04	99.61	80.87
XD10-(2)-4B	52.02	2.25	13.17	10.55	0.10	9.14	8.15	3.15	0.90	0.38	0.04	99.84	78.72
XD10-(2)-5	51.04	2.08	13.40	11.70	0.12	8.82	7.81	3.28	0.90	0.36	0.05	99.56	80.82
XD10-(3)-1	50.15	1.94	11.83	14.69	0.14	8.75	6.70	3.12	0.79	0.33	0.03	98.47	73.01
XD-10(3)-1-R	50.63	1.96	12.08	14.68	0.15	8.67	6.83	2.96	0.70	0.32	0.03	98.99	73.01
XD10-(3)-1-RR	50.39	1.95	11.95	14.69	0.15	8.71	6.76	3.04	0.74	0.33	0.03	98.73	73.01
XD10-(3)-2	49.74	2.28	12.77	14.86	0.15	7.60	8.11	3.18	0.76	0.34	0.02	99.81	80.61
XD10-(3)-4B	50.40	2.02	11.77	15.46	0.16	7.81	7.43	2.94	0.93	0.36	0.04	99.31	71.08
XD10-(3)-5	51.84	2.25	13.53	9.26	0.11	9.59	8.53	3.21	0.96	0.39	0.04	99.71	81.18
XD10-(3)-6A	51.07	2.12	13.50	11.63	0.13	9.08	7.88	3.22	0.86	0.35	0.04	99.88	78.06
XD-10(3)-6B	51.31	2.28	13.66	11.21	0.12	8.80	8.30	3.14	0.76	0.35	0.03	99.95	77.29
XD10-(3)-7/A	51.05	2.24	13.37	10.52	0.11	9.34	7.98	3.19	0.89	0.35	0.04	99.07	80.23
XD10-(4)-1	50.23	2.02	12.98	13.34	0.15	9.32	7.24	3.27	0.93	0.36	0.03	99.87	77.10
XD10-(4)-2A	51.84	2.33	12.33	12.39	0.13	8.80	7.22	3.13	1.13	0.38	0.05	99.74	74.07
XD10-(4)-3/	49.17	2.05	12.38	15.82	0.16	8.83	7.34	2.99	0.83	0.35	0.04	99.95	72.28
XD10-(4)-3A	50.22	2.25	12.73	14.79	0.17	7.27	7.50	3.22	0.97	0.42	0.01	99.55	73.83
XD10-(4)-3B	49.22	1.97	11.88	17.84	0.20	7.58	6.95	3.01	0.82	0.46	0.02	99.93	72.68
XD10-(4)-4	50.78	2.06	12.58	12.83	0.14	8.78	7.59	3.26	0.91	0.36	0.04	99.34	78.43
XD10-(4)-5A	51.78	2.13	12.81	11.31	0.12	8.74	8.28	3.38	0.90	0.35	0.05	99.84	79.04
XD10-(4)-5B	50.89	2.20	12.91	12.08	0.12	8.51	8.49	3.32	0.85	0.35	0.04	99.76	78.72
XD10-(4)-6A	49.82	2.18	12.73	14.30	0.14	8.25	7.77	3.19	0.83	0.35	0.03	99.58	73.33
XD10-(4)-7	50.02	2.09	12.47	14.95	0.14	8.31	7.35	3.18	0.83	0.37	0.02	99.74	76.52
XD10-(5)-1	49.54	2.20	12.91	14.98	0.15	7.64	7.67	3.26	0.84	0.43	0.03	99.65	77.98
XD10-(5)-2	50.05	2.19	14.07	11.53	0.13	9.26	8.18	3.29	0.84	0.36	0.04	99.93	82.05
XD10-(5)-3	48.23	1.98	12.76	15.82	0.15	8.73	7.69	3.01	0.82	0.35	0.03	99.58	77.29
XD10-(5)-4	51.00	2.16	14.02	9.79	0.09	9.77	8.14	3.26	0.96	0.37	0.05	99.59	79.26
XD10-(5)-5A	50.46	2.10	12.61	13.88	0.13	8.56	7.55	3.10	0.86	0.36	0.05	99.66	78.11
XD10-(5)-5B	50.71	2.06	13.24	12.39	0.12	8.82	7.72	3.18	0.92	0.35	0.05	99.56	78.11
XD10-(5)-6	50.11	2.10	13.08	13.39	0.14	8.46	8.00	3.13	0.92	0.34	0.05	99.73	75.59

fractionation. During olivine fractionation, FeO contents in basaltic melts are relatively constant, due to its partition coefficient between olivine and melt equaling to unity. Thus, we assume a constant FeO content during the Fe-loss correction. We used the method of Danyushevsky et al. (2000) and the model of Ford et al. (1983) for "Fe-loss" correction and post-crystallization, by assuming the total FeO contents of Xindian lavas to be 10.9 wt%, and oxygen fugacity to be QFM. On a total alkalis-silica (TAS) diagram (Fig. 3), both bulk rocks and melt inclusions after correction are tholeiitic. MgO contents of melt inclusions after correction are from 4.8 to 8.6 wt% (Fig. 4), lower but wider than those of melt inclusions without correction. In Fig. 4, with decreasing MgO contents, SiO_2, TiO_2, Al_2O_3, CaO and Na_2O contents generally increase, and CaO/Al_2O_3 ratios are relatively constant at MgO > 6 wt%, indicating olivine as the dominant crystallizing phase. Slightly positive correlations between MgO and Al_2O_3, and MgO and CaO, and a negative correlation between MgO and CaO/Al_2O_3 ratios are observed at MgO < 5.5 wt%, indicating

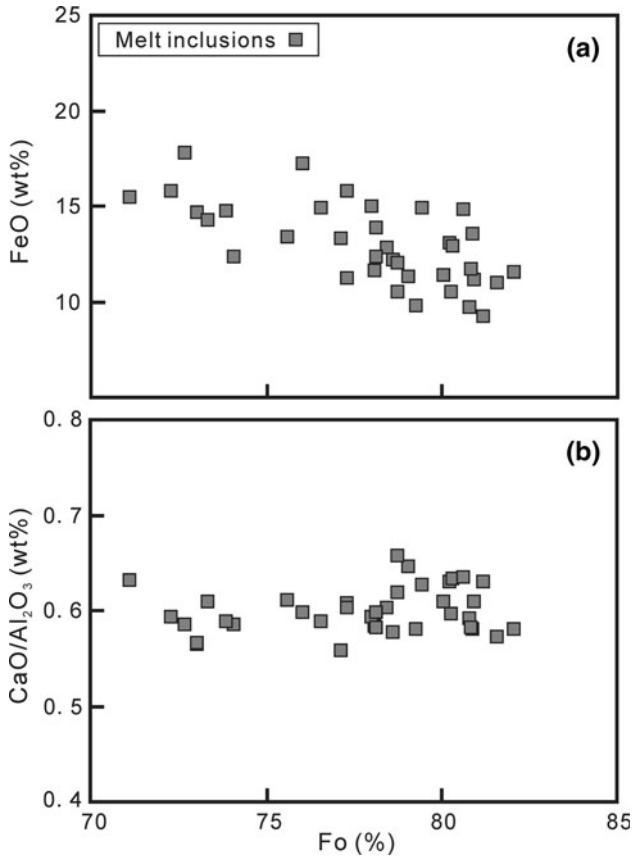

Fig. 2 **a** The plot of FeO contents of melt inclusions in Xindian basalts against Fo values of their host olivines. "Fe-loss" is expressed as a slightly negative relationship illustrated in **a**. **b** The plot of CaO/Al_2O_3 ratios of melt inclusions versus Fo of their host olivines. The relatively constant CaO/Al_2O_3 ratios suggest no obvious clinopyroxene and plagioclase fractionation

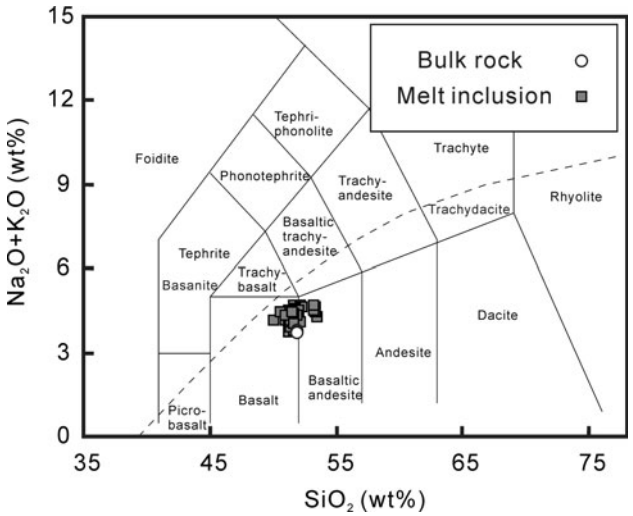

Fig. 3 TAS diagram after Le Bas et al. (1986) for bulk rocks and melt inclusions of Xindian basalts. The compositions of melt inclusions are corrected after Fe-loss (see text further explanation). The bulk compositions are normalized volatile-free, after total Fe contents are divided into FeO and Fe_2O_3 via assuming Fe^{2+}/Fe^{3+} to be 9.0

that plagioclases crystallize from the magma. An interesting phenomenon is that when MgO contents are between 5.5 and 6.0 wt%, Al_2O_3 contents show a negative correlation with MgO, whereas CaO contents exhibit a slightly positive correlation with MgO. As CaO/Al_2O_3 ratios remain constant, we infer that this difference is due to the more scatter of CaO contents at a given MgO.

The variation of trace element compositions of Xindian basalts is also limited, with La/Yb ratios ranging from 10.6 to 11.7 (Table 1). Their trace element distribution patterns (Fig. 5) resemble those of typical EMI OIBs, characterized by enrichment of large ion lithophile elements (LILEs), positive anomalies of Ba, Ta and Sr, but no significant anomalies of high field strength elements (HFSEs, such as Nb, Zr–Hf and Ti; Fig. 5).

Olivine compositions

Fo values in Xindian olivine crystals are relatively low (ranging from 71.0 to 82.1, Table 3), and CaO contents in olivines are higher than 0.15 wt% (Fig. 6). CaO contents remain nearly constant at Fo > 75 and gradually increase with decreasing Fo when Fo < 75 (Fig. 6). MnO and NiO contents of the Xindian olivines range from 0.20 to 0.31 wt%, and from 0.19 to 0.35 wt%, respectively. They show negative and positive correlations with Fo, respectively (Fig. 7b, c). Fe/Mn ratios of olivines are higher than 80 and exhibit no correlation with Fo (Fig. 7d). Compared with those crystallizing from peridotite melts, olivine crystals in Xindian basalts are characterized by lower Ca and Mn contents, but higher Ni contents and Fe/Mn ratios at a given Fo value (Fig. 7).

Discussion

Olivine phenocrysts or xenocrysts?

There are two types of olivine crystals in basaltic lavas: phenocrysts crystallized from magma and mantle-derived xenocrysts. Based on the following observations, we conclude that all olivines in this study are phenocrysts. In thin sections, olivine crystals (>0.5 mm) generally appear with euhedral and subhedral shapes, which are different from most mantle xenocrysts with the anhedral profiles (e.g., Kamenetsky et al. 2006). In addition, CaO contents of the Xindian olivines are higher than 0.1 wt% (Fig. 6), consistent with a derivation from magmas (Simkin and Smith 1970; Garcia et al. 1995; Ren et al. 2004). Besides, Fo values in olivines in Xindian basalts are relatively low (Fo < 85), compared with those of mantle xenoliths from

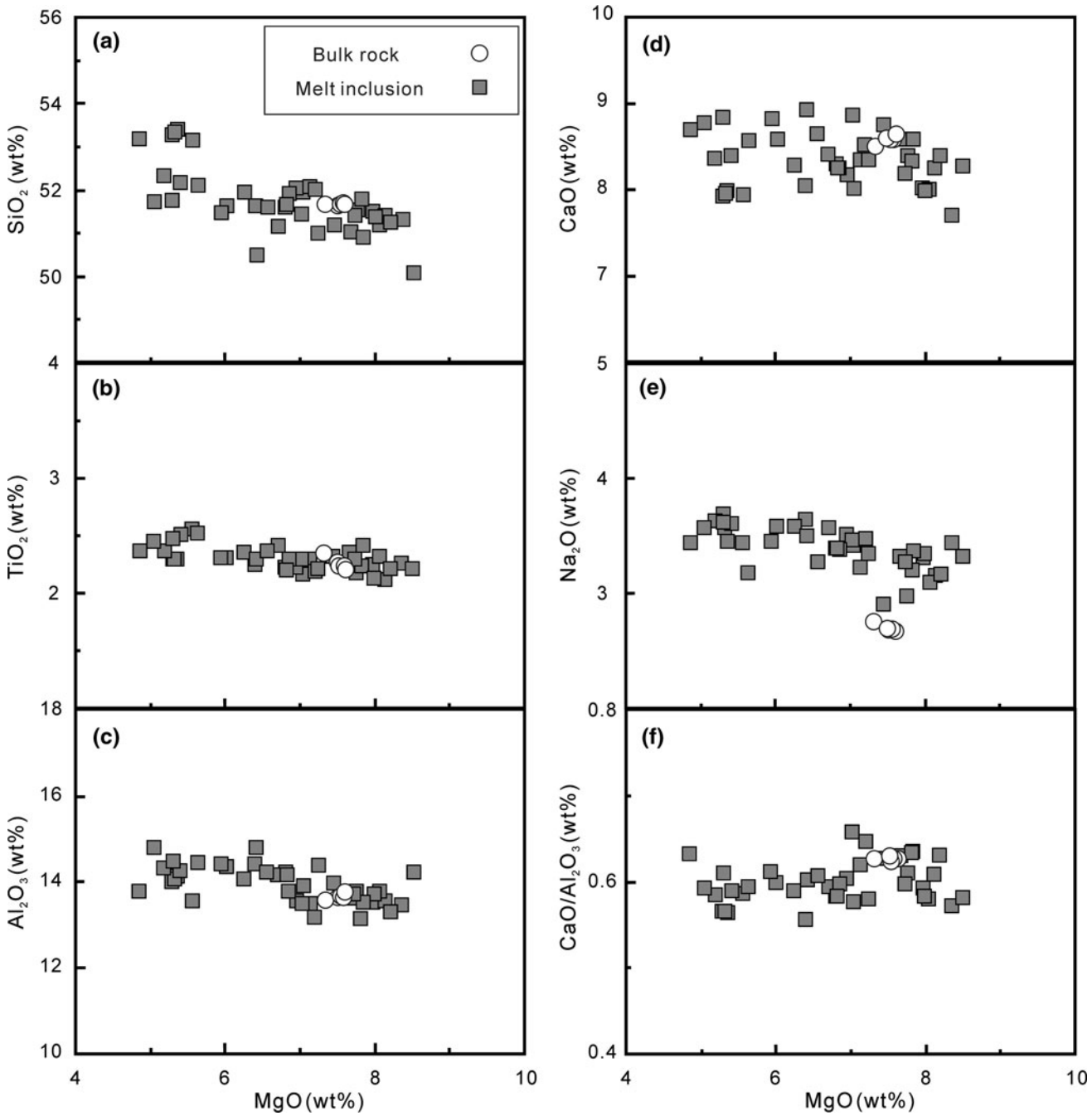

Fig. 4 Major element contents and their ratios against MgO variation diagrams for bulk rocks and melt inclusions of Xindian basalts after correction for Fe-loss: **a** SiO_2 versus MgO; **b** TiO_2 versus MgO; **c** Al_2O_3 versus MgO; **d** CaO versus MgO; **e** Na_2O versus MgO; **f** CaO/Al_2O_3 versus MgO. The data are consistent with those in Fig. 3. Note that the bulk rocks plot in the field of melt inclusions, except Na_2O versus MgO, indicating they are co-genetic. Lower Na_2O contents of bulk rocks might be due to alteration after eruption

eastern NCC (mostly Fo > 89; Fan and Hooper 1989; Zheng et al. 1998, 2001, 2006; Fan et al. 2000; Rudnick et al. 2004; Xu and Bodinier 2004; Yang et al. 2008; Chu et al. 2009; Xia et al. 2010; Xiao et al. 2010). Furthermore, melt inclusions hosted by Xindian olivines are mostly isolated and thus original, in contrast with the absence of original melt inclusions in olivine xenocrysts (Schiano 2003). More importantly, compositional variation of melt inclusions is generally consistent with the trend of fractional crystallization on which bulk rocks also fall (Figs. 4, 8), further supporting the conclusion that olivines in this study are magmatic in origin.

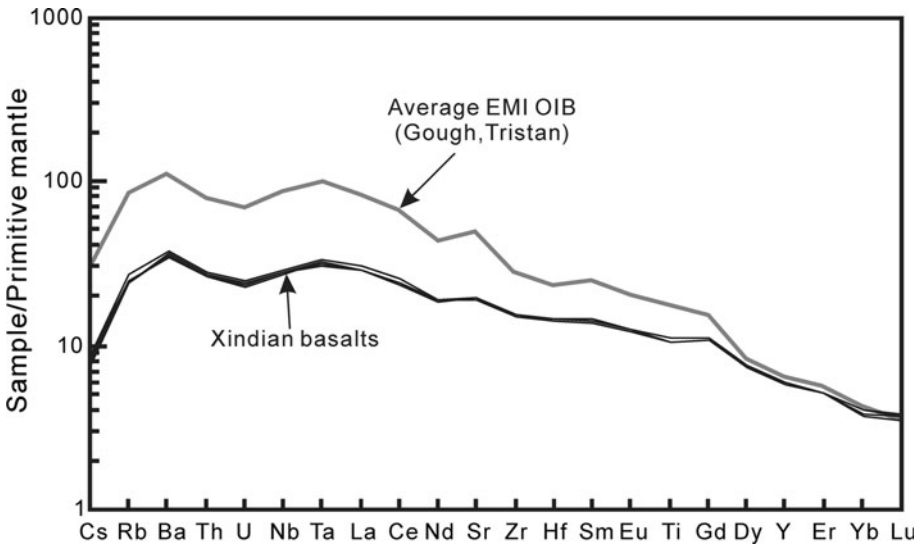

Fig. 5 Primitive mantle (McDonough and Sun 1995)-normalized trace element patterns for Xindian basalts. The average data of EMI OIB are from Willbold and Stracke (2006)

Evolution of Xindian basalts

Alteration and crustal contamination?

Magmas might undergo alteration after eruption on the surface, or crustal contamination during magma ascent through the whole crust. Thus, it is important to assess the effect of alteration and crustal contamination before discussing the crystallization and petrogenesis of the magmas.

Although iddingsites are present in some olivines, most olivines are rather fresh. In addition, LOI values of the Xindian basalts are all very low (<0.01 wt%; Table 1), some even below zero (Table 1). The negative values indicate that the increased weight via oxidation of FeO to Fe_2O_3 is heavier than the lost weight via losing volatiles. Although the estimation of the effect of crustal contamination is hard, due to the similar compositions of five studied samples, lack of significant negative anomalies of HFSEs (Nb–Ta, Zr–Hf and Ti) in primitive mantle-normalized trace element patterns (Fig. 5) is indicative of insignificant crustal contamination on Xindian basalts.

Crystallization

Rather, limited bulk rock compositions of the Xindian basalts make it impossible to discuss the crystallization of magmas. Here we try to reconstruct the crystallization process of Xindian basalts, using melt inclusion compositions. Olivine is the main phenocryst phase of the Xindian basalts, with minor plagioclase phenocrysts. The matrix of Xindian basalts is composed of plagioclase, clinopyroxene, olivine and ilmenite. All these suggest that olivine and plagioclase crystallize earlier than clinopyroxene and ilmenite.

On the Harker diagram (Fig. 4), with decreasing MgO, CaO and Al_2O_3 of melt inclusions increase at MgO $> \sim$6.0 wt%, whereas they decrease slightly at MgO $<$ 5.5 wt%. CaO/Al_2O_3 ratios remain constant at MgO $> \sim$5.5 wt%, but increase slightly at MgO $< \sim$5.5 wt%. Thus, we deduce that olivine is the primary phenocryst phase at MgO $> \sim$5.5 wt%, and plagioclase might begin to crystallize at MgO $= \sim$5.5 wt%. Clinopyroxene is not a liquidus phase at MgO $>$ 5.0 wt%.

Given the low MgO contents of melt inclusions (all <8.6 wt%), it is necessary to discuss whether clinopyroxene and plagioclase participate the crystallization process at higher MgO. Rare and small plagioclase phenocrysts in thin sections indicate that positive anomaly of Sr in Fig. 5 possibly inherits from the source, rather than plagioclase accumulation. Clinopyroxene fractionation at higher MgO contents is hard to assess. Yet, several traces hint clinopyroxene could not crystallize too early. (1) No clinopyroxene phenocrysts are observed in thin sections. (2) Sc contents of Xindian basalts ($\sim$20 ppm) are comparable to those of other Cenozoic high MgO basalts (MgO $>$ 11 wt%) in eastern China (Sc 16–27 ppm; Fan and Hooper 1991). This rules out the possibility of significant clinopyroxene fractionation in the Xindian case, which would have significantly lowered Sc contents in residual melts because of its compatibility in clinopyroxene. (3) Modeling calculation using MELTS shows that the magma chamber pressure of the Xindian basalts is relatively low ($P \leq$ 1,000 bar; Fig. 8d, f). At such low pressure, clinopyroxene crystallization is impossible.

Therefore, we infer that the order of crystallized minerals of the Xindian basalts is as follows: olivine (at MgO $>$ 5.5 wt%), plagioclase (beginning at MgO $= \sim$5.5 wt%), clinopyroxene and ilmenite (both at MgO $<$ 5.0 wt%).

Table 3 Major and minor element compositions of olivine phenocrysts of Xindian basalts analyzed by EPMA

	SiO_2	FeO	MnO	MgO	CaO	NiO	Total	Fo
XD10-(1)-1	39.61	17.74	0.20	41.78	0.18	0.33	99.83	80.76
XD10-(1)-2	38.92	21.74	0.25	38.61	0.17	0.28	99.96	76.00
XD10-(1)-3A	37.95	22.71	0.24	37.96	0.17	0.21	99.25	74.87
XD10-(1)-3B	38.40	21.27	0.22	38.73	0.17	0.23	99.02	76.45
XD10-(1)-3C	38.25	21.54	0.23	39.01	0.20	0.24	99.47	76.35
XD10-(1)-4	38.43	23.54	0.27	36.96	0.21	0.23	99.64	73.67
XD10-(1)-5	39.85	18.46	0.22	40.89	0.18	0.33	99.93	79.80
XD10-(1)-6A	39.30	19.47	0.22	40.07	0.18	0.32	99.56	78.58
XD10-(1)-6B	39.23	18.86	0.22	40.81	0.18	0.31	99.61	79.41
XD10-(1)-7	39.33	18.24	0.22	41.44	0.19	0.31	99.73	80.20
XD10-(2)-1	39.56	17.01	0.20	42.13	0.19	0.35	99.44	81.54
XD10-(2)-1/A	39.29	18.18	0.21	41.29	0.19	0.34	99.49	80.20
XD10-(2)-1/B	39.40	18.35	0.20	41.28	0.19	0.34	99.77	80.04
XD10-(2)-1/C	39.78	17.49	0.20	41.56	0.19	0.34	99.55	80.90
XD10-(2)-2	39.35	18.07	0.21	41.26	0.19	0.33	99.41	80.27
XD10-(2)-3	39.79	17.55	0.20	41.61	0.19	0.34	99.69	80.87
XD10-(2)-4A	39.36	21.27	0.26	38.21	0.20	0.29	99.59	76.20
XD10-(2)-4B	39.54	19.33	0.22	40.11	0.20	0.33	99.73	78.72
XD10-(2)-4C	38.99	20.96	0.25	39.25	0.19	0.30	99.93	76.95
XD10-(2)-5	39.45	17.66	0.21	41.75	0.18	0.35	99.60	80.82
XD10-(2)-6	39.00	20.80	0.24	39.30	0.18	0.29	99.81	77.11
XD10-(2)-7	39.60	17.95	0.22	41.64	0.19	0.35	99.94	80.52
XD10-(3)-1	38.34	23.88	0.27	36.24	0.18	0.22	99.13	73.01
XD10-(3)-2	39.95	17.65	0.21	41.16	0.18	0.34	99.49	80.61
XD10-(3)-2/A	39.17	21.65	0.26	37.88	0.19	0.26	99.40	75.72
XD10-(3)-2/B	39.66	18.03	0.20	41.35	0.18	0.34	99.76	80.35
XD10-(3)-3	38.80	21.37	0.24	38.48	0.17	0.26	99.31	76.25
XD10-(3)-4B	38.79	25.40	0.31	35.02	0.20	0.21	99.93	71.08
XD10-(3)-5	40.12	17.07	0.20	41.31	0.18	0.35	99.23	81.18
XD10-(3)-6A	40.15	19.49	0.24	38.89	0.19	0.29	99.24	78.06
XD10-(3)-6B	39.26	20.42	0.23	38.99	0.18	0.28	99.35	77.29
XD10-(3)-7	39.90	17.67	0.20	41.32	0.18	0.33	99.60	80.65
XD10-(3)-7/A	39.67	18.05	0.20	41.09	0.19	0.34	99.53	80.23
XD10-(3)-7/B	39.54	17.86	0.20	41.35	0.19	0.34	99.49	80.50
XD10-4-1	38.82	20.71	0.23	39.12	0.18	0.30	99.35	77.10
XD10-4-2A	39.16	22.78	0.27	36.50	0.20	0.28	99.18	74.07
XD10-4-2B	39.42	17.71	0.19	41.49	0.19	0.34	99.34	80.68
XD10-4-3A	38.63	23.45	0.29	37.12	0.18	0.21	99.86	73.83
XD10-4-3B	38.46	24.13	0.29	36.02	0.19	0.21	99.30	72.68
XD10-4-3/	38.15	24.74	0.30	36.18	0.22	0.19	99.77	72.28
XD10-4-4	39.22	19.47	0.23	39.73	0.18	0.33	99.16	78.43
XD10-4-4/	38.36	25.52	0.31	35.34	0.19	0.22	99.93	71.17
XD10-4-5A	39.15	19.04	0.22	40.29	0.17	0.33	99.20	79.04
XD10-4-5B	39.54	19.21	0.23	39.88	0.18	0.33	99.37	78.72
XD10-4-6A	38.83	23.65	0.28	36.49	0.20	0.22	99.68	73.33
XD10-4-6B	38.59	23.06	0.28	37.19	0.21	0.24	99.56	74.20
XD10-4-7	39.13	21.16	0.26	38.70	0.18	0.27	99.69	76.52
XD10-5-1	39.16	20.02	0.24	39.77	0.19	0.30	99.67	77.98

Table 3 continued

	SiO_2	FeO	MnO	MgO	CaO	NiO	Total	Fo
XD10-5-2	39.99	16.54	0.20	42.42	0.18	0.35	99.68	82.05
XD10-5-3	38.43	20.59	0.24	39.31	0.18	0.29	99.03	77.29
XD10-5-4	39.12	18.94	0.22	40.62	0.18	0.34	99.42	79.26
XD10-5-5A	38.67	20.03	0.24	40.10	0.18	0.30	99.52	78.11
XD10-5-6	38.69	21.97	0.25	38.15	0.18	0.26	99.50	75.59

Pyroxenite source or peridotite source?

Olivine chemistry: a review

Sobolev et al. (2005) found that Ni contents of olivines in high SiO_2 Hawaii basalts were unusually high and argued them derived from pyroxenite melts. Later, Sobolev et al. (2007) further investigated the compositions of olivine phenocrysts in various magmas from different tectonic setting. They found that most olivine phenocrysts from MORB and many from komatiites had Mn and Ni contents comparable with those of peridotite melts. However, olivine phenocrysts from tholeiitic and transitional magmas of OIB and LIP emplaced on thick lithosphere (WPM-THICK group) had generally higher Ni and Fe/Mn, but lower Ca and Mn, which was explained as the result of higher proportion of pyroxenite melts in WPM-THICK group.

However, the pyroxenite model, proposed by Sobolev and his colleagues, aroused hot debates (e.g., Niu and O'Hara 2007; Niu et al. 2011; Herzberg 2011; Putirka et al. 2011; Rhodes et al. 2012). Niu and his coworkers explained the first-order correlation between olivine compositions and thickness of lithosphere as the result of the lid effect rather than the original source composition (e.g., Niu and O'Hara 2007; Niu et al. 2011). They argued that the high Ni contents and Fe/Mn ratios of olivine phenocrysts from the thick lithosphere were due to their high corresponding values of the melt formed at high pressure. They thought that at high pressure, olivines consumed and high MgO melts produced would increase Ni contents in the primitive melts, and garnet occurring in the residual source would low Fe/Mn ratios in the melt. Alternatively, Putirka et al. (2011) emphasized the role of temperature on the partition coefficient. They argued that due to higher $D_{Ni}^{ol\text{-}melt}$ at lower temperature, Ni contents of the olivine phenocrysts crystallizing at relatively low temperature would be higher than those of mantle materials in the residual source. They held that the higher Ni contents in Koolau olivines were probably due to the lower crystallization temperature. They further pointed out melting of peridotites with the median Ni contents could yield the high Ni contents of Hawaii melts, and the high Ni olivines may be due to the elevated temperature of peridotite melting.

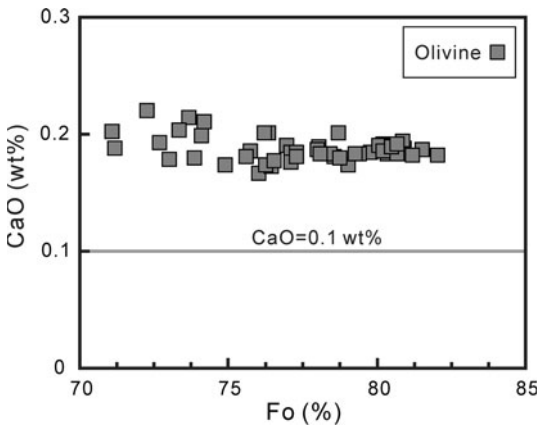

Fig. 6 Diagram of CaO contents against Fo values for olivines of Xindian basalts. Note that CaO contents of all olivines of Xindian basalts are higher than 0.1 wt%, suggesting their magmatic origin

Herzberg (2011) modeled the composition variation of olivines (such as Ni, Ca, Mn and Fe/Mn) from fertile peridotite melts (the plot of Herzberg 2011; Fig. 7) and applied the modeling results to the natural samples. He found that compositions of olivines in MORB and Alexo komatiites were consistent with the expected olivine compositions of peridotite melts, thus suggesting a peridotite source for these lavas. They argued that Koolau lavas were pyroxenite melts, in view of higher Ni and Fe/Mn and lower Ca and Mn of olivines. They further pointed out that both pyroxenite and peridotite occurred in the source of Loihi lavas.

Recently, Rhodes et al. (2012) reported that the Ni contents between low and high SiO_2 lavas from Mauna Kea shield were comparable, thus casting doubt on the pyroxenite model. They argued that following the method of Sobolev et al. (2005), the Ni contents of primitive peridotite melts resemble those of Mauna Kea lavas, when $D_{Ni}^{ol\text{-}melt}$ of Putirka et al. (2011) instead of Beattie et al. (1991) was applied. They also found that even using $D_{Ni}^{ol\text{-}melt}$ of Beattie et al. (1991), melting of peridotite with a little higher Ni content (e.g., 2,200 ppm) in the source would also yield similar Ni contents of Mauna Kea lavas. Thus, Rhodes et al. (2012) concluded that because of the uncertainty in either Ni content of peridotite source or the $D_{Ni}^{ol\text{-}melt}$, the model of Sobolev et al. (2005) was not persuasive.

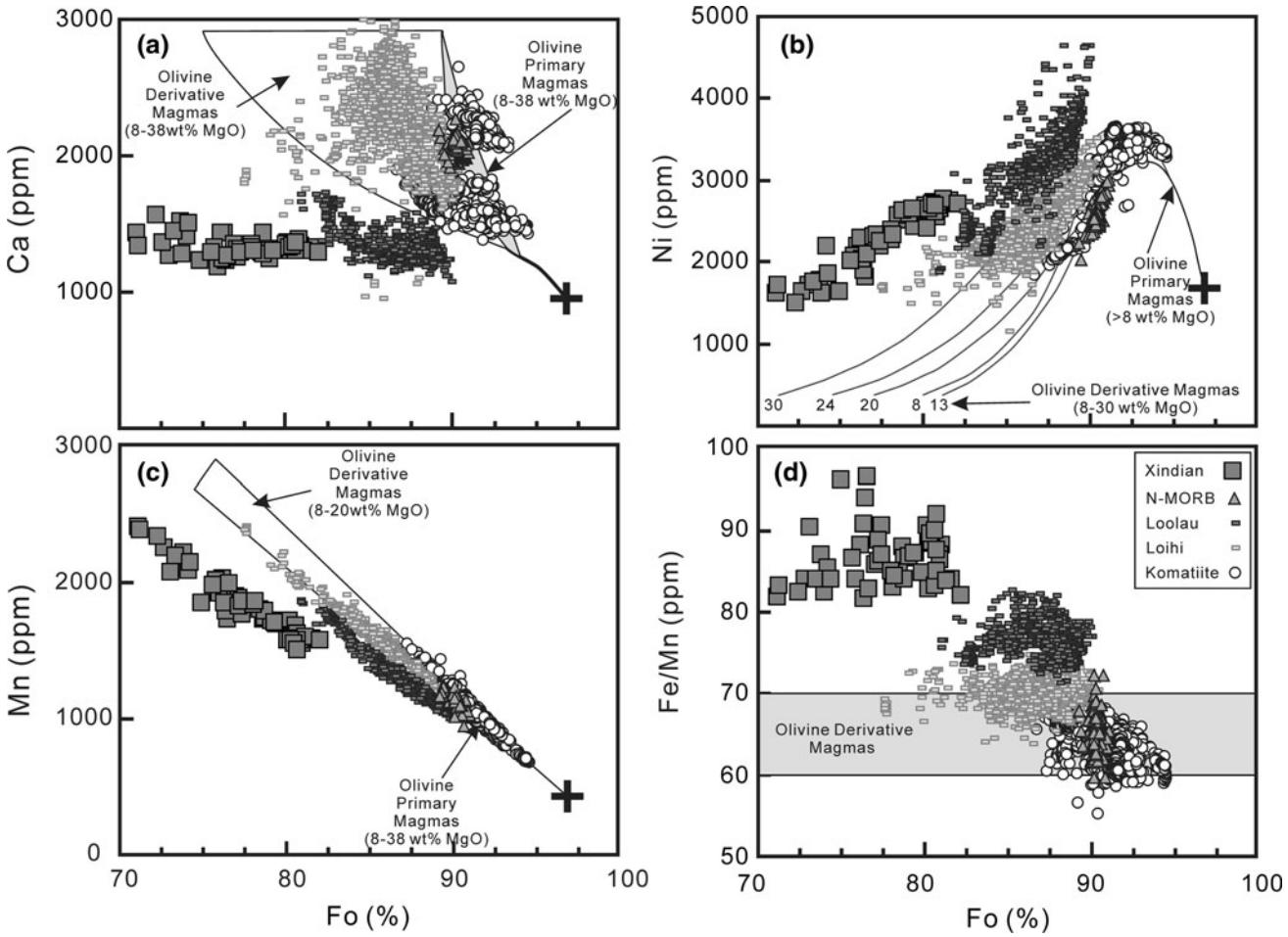

Fig. 7 Plots of Ca (**a**), Ni (**b**), Mn (**c**) and Fe/Mn (**d**) against Fo for olivines of Xindian basalts. The corresponding compositions of olivines crystallizing from peridotite melts after Herzberg (2011) are also shown. Data source of olivines in komatiites worldwide, Loihi lavas and Koolau lavas is from Sobolev et al. (2007). Data source of olivines in N-MORB from Siqueiros is from Sobolev et al. (2007) and Putirka et al. (2011)

Olivine chemistry of Xindian basalts

Although identification of the source lithology based on the olivine phenocrysts is still problematic, the plot of Herzberg (2011) is a good test. Since several factors, including the lid effect (corresponding to the melting pressure; Niu et al. 2011), the melting temperature (Putirka et al. 2011), the partition coefficients between olivine and melt, and compositions in the mantle source (Putirka et al. 2011; Rhodes et al. 2012), can affect the compositions of olivine phenocrysts, it is necessary to examine the validity of the plot before projecting olivine data of Xindian basalts.

We choose various natural peridotite melts (komatiites from worldwide, Loihi lavas and N-MORB from Siqueiros), with melting pressures from >7.0 GPa to <2.0 GPa (e.g., Kinzler and Grove 1992a, b; Walter 1998), and melting temperatures from anomalously high to normal mantle potential temperature (e.g., McKenzie and O'Nions 1991; Putirka 2005). These melts chosen in random will also effectively erase the influence of compositions in mantle source and check the partition coefficient. In Fig. 7, olivine compositions from these melts generally plot well in the fields of expected olivine compositions from peridotite melts, suggesting that the plot is valid for peridotite melts.

In the plot of Herzberg (2011), Ni and Fe/Mn of olivines in Xindian basalts are higher, but Ca and Mn are lower than those of olivines in peridotite melts at a given Fo (Fig. 7). Similar olivine compositions are reported in Koolau lavas (Fig. 7; Sobolev et al. 2007; Herzberg 2011). Although some researchers argued that high Ni olivines in Koolau lavas could crystallize from peridotite melts (Putirka et al. 2011; Rhodes et al. 2012), several lines of evidences suggest that peridotite as the source lithology of Koolau lavas seems impossible. (1) Assuming peridotite as the source of the whole Hawaii lavas (e.g., Putirka et al. 2011; Rhodes et al. 2012), Koolau and Loihi lavas would possibly have similar Ni contents, due to the comparable $D_{Ni}^{ol\text{-}melt}$ values

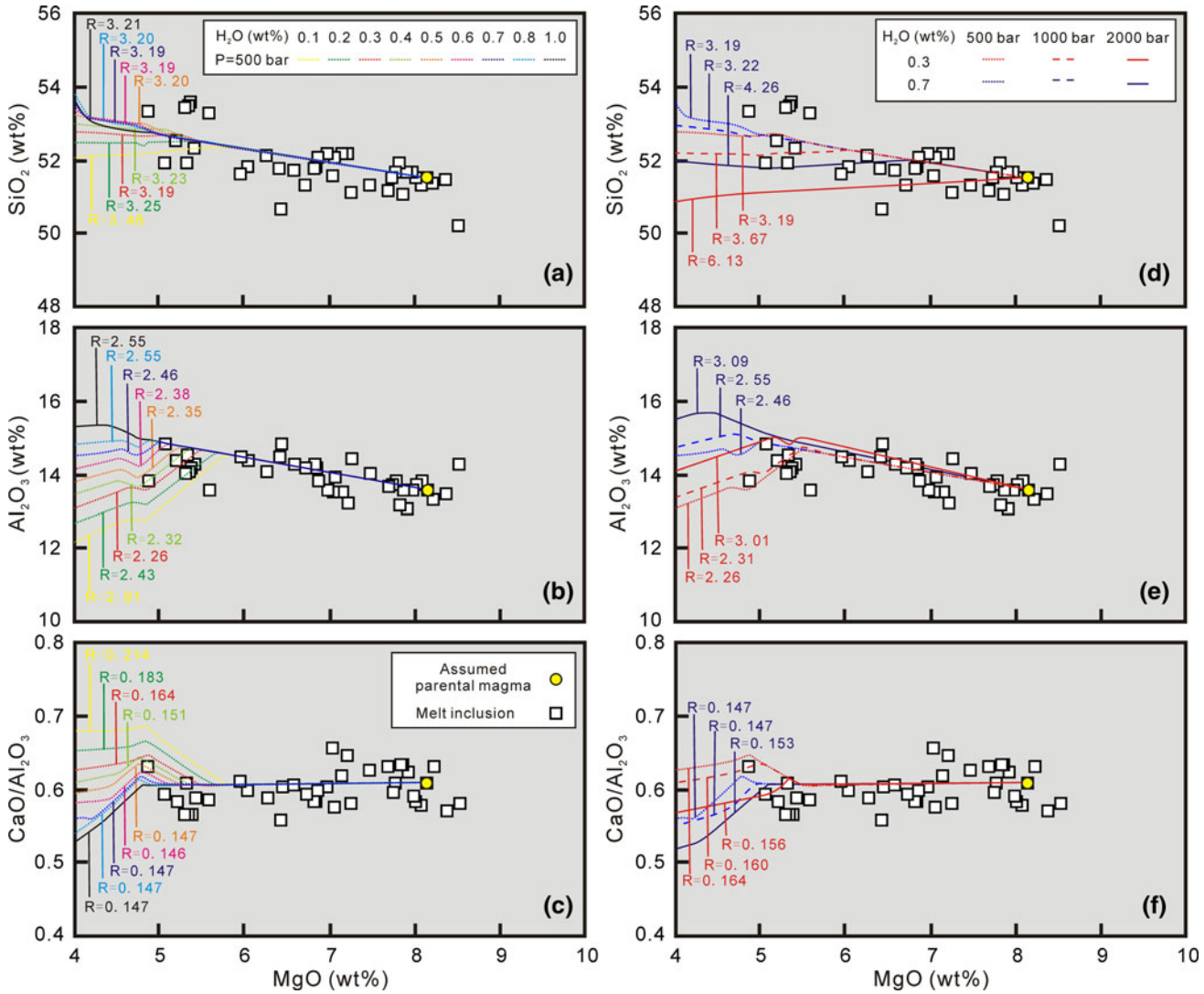

Fig. 8 Comparison of the crystallization trends of melt inclusions of Xindian basalts after Fe-loss correction and the calculated fractional crystallization trends using MELTS program by assuming a high MgO melt inclusion (MgO = 8.13 wt%) as a parental magma. R shown in the diagrams, a parameter reflecting the degree of deviation from the data, is the square root of the sum of squares of difference between model liquid lines of descent (LLD) and data points at equal MgO. The *left diagrams* (**a**–**c**) for various water contents in the melts at given pressure (500 bar). Note that the modeled LLD of 0.3–0.7 wt% water contents best fit the data points, as evidenced from the lowest R values in these three diagrams. The *right diagrams* (**d**–**f**) for different pressures (500, 1,000 and 2,000 bar, respectively) at given water contents in the melts (0.3 wt% and 0.7 wt%, respectively). Note that with increasing pressures, the deviation of the modeled LLD from the data points increases, indicating that the crystallization pressure is very low (no more than 1,000 bar)

and Ni contents in the source. Thus, compositions of olivine phenocrysts would be similar. Yet, Koolau lavas have higher Ni and Fe/Mn, but lower Mn and Ca of olivines than Loihi lavas. According to Putirka et al. (2011), higher Ni olivines in Koolau lavas is possibly due to the lower crystallization temperature. Following this reasoning, the lower crystallization temperature in Koolau lavas would result in lower Ni contents in low Fo olivines (see Fig. 5a in Putirka et al. 2011), an expectation not observed (Fig. 7). (2) Koolau lavas are dominated by silica-excess melts (e.g., Herzberg 2011), which could not be directly derived from silica-deficient source, for example, peridotite, at high pressure (Kogiso et al. 2004). Putirka et al. (2011) proposed that the reaction between the high-pressure peridotite melt and harzburgite at low pressure, similar to the model of Wagner and Grove (1998), could explain the high SiO_2 content of Koolau lavas. However, such reaction would result in olivine crystallization, thus lowering Ni contents of lavas and olivine phenocrysts, which contradicts the fact of the high Ni olivines in Koolau lavas. (3) Compared with other lavas in Hawaii, Koolau lavas have anomalously low CaO contents at given MgO content (Herzberg 2011; Putirka et al. 2011). Although the high-pressure (3.0 GPa) peridotite melts could share similar CaO contents at given MgO

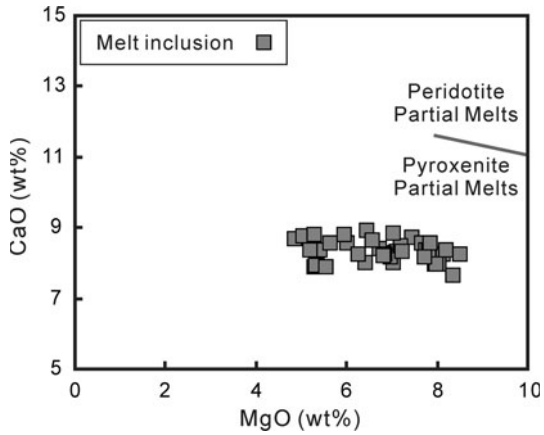

Fig. 9 Diagram of CaO against MgO for melt inclusions of Xindian basalts after Fe-loss correction. The divide line of pyroxenite melts and peridotite melts after Herzberg and Asimow (2008) is also shown

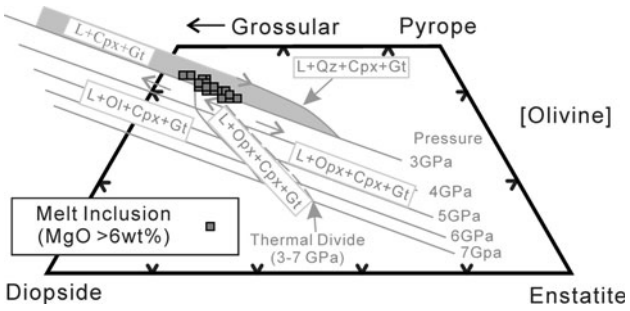

Fig. 10 CS-MS-A diagram after Herzberg (2011) for the high MgO contents of melt inclusions (MgO > 6.0 wt%) of Xindian basalts after Fe-loss correction. The detailed description of CS-MS-A diagram can be seen in Herzberg (2006, 2011). Note that all the melt inclusions plot in the field between L + Cpx + Gt and L + Cpx + Opx + Gt at ~3.0 GPa. This means that the residual minerals after melt extraction from the source of Xindian basalts are mainly Cpx and Gt, possibly Opx, but no Ol, and the melting pressure possibly reaches ~3.0 GPa

(Longhi 2002; Putirka et al. 2011), such low CaO peridotite melts would also have lower SiO_2 content at given MgO (Fig. 6 (a) and (b) in Putirka et al. 2011). Putirka et al. (2011) also proposed a mixture melt by various high-pressure peridotite melts equilibrating with harzburgite at relatively low pressure (1–1.5 GPa) for the parental melts of Koolau lavas. However, as discussed before, such mixing melts fail to explain the high Ni olivines in Koolau lavas. Therefore, we hold that the pyroxenite is the source of Koolau lavas (Ren et al. 2004, 2005, 2006, 2009; Sobolev et al. 2005; Herzberg 2011), consistent with the conclusion made on their special olivine compositions (Fig. 7). Given the fact that olivine compositions of Xindian basalts are similar to those of Koolau lavas (Fig. 7), we thus prefer the pyroxenite as the source of Xindian basalts.

Melt inclusion chemistry

Only melt inclusions with MgO > 6.0 wt% are used to constrain the source lithology of Xindian basalts, because they were only subjected to olivine fractionation. In the CaO–MgO diagram (Fig. 9), the Xindian melt inclusions have low CaO contents and project in the field of pyroxenite melts, again indicating a pyroxenite source for the Xindian basalts (Herzberg 2006; Herzberg and Asimow 2008). Furthermore, in the CS-MS-A diagram, these melt inclusions plot in the field between Opx + Cpx + Gt + L and Cpx + Gt + L at ~3.0 GPa (Fig. 10), further indicating that the residual minerals are mainly clinopyroxene and garnet, possibly in the presence of minor orthopyroxene but without olivine, and the melting depth is ~3.0 GPa (Herzberg 2006, 2011). Such an inference is in accordance with the high Ni and Fe/Mn, and low Ca and Mn in olivines of the Xindian basalts.

Another important evidence in favor of a pyroxenite source for the Xindian basalts is that if assuming the source is peridotite, using PRIMELT2 program (Herzberg and Asimow 2008), the MgO contents of the primitive magmas of nearly all high MgO melt inclusions (MgO > 6 wt%) are higher than 20 wt%, which is unreasonable (not shown). The best explanation is that the source of Xindian basalts is the Fe-rich source, such as pyroxenite.

Summary

Olivine chemistry has the potential ability to identify the source lithology. Comparing with those peridotite melts, olivine phenocrysts of Xindian basalts bear higher Ni contents and Fe/Mn ratios, but lower Ca and Mn contents at a given Fo value, and high MgO melt inclusions have lower CaO contents at a given MgO content, both suggesting that the pyroxenite is the possible source of Xindian basalts. In the CS-MS-A diagram, nearly all high MgO melt inclusions fall in the field between L + garnet + clinopyroxene and L + garnet + clinopyroxene + orthopyroxene near 3.0 GPa, further constraining that the residual minerals in the source after melt extraction are mainly garnet and clinopyroxene, possibly in the presence of a little orthopyroxene, but no olivine. Therefore, our study clarifies that not only alkali basalts but also tholeiitic basalts in the NCC are possibly derived from the pyroxenite source.

The formation of pyroxenite and melting degrees of Xindian basalts

Pyroxenite could exist either in asthenospheric or in lithospheric mantle. We prefer asthenospheric pyroxenite as the source of the Xindian basalts, following two main reasons. The initial ε_{Nd} values ($\varepsilon_{Nd(t)}$) of mafic magmas in

the whole eastern NCC increase gradually from $\varepsilon_{Nd(t)} < 0$ in Late Mesozoic to $\varepsilon_{Nd(t)} > 0$ in Cenozoic (Xu 2001). The mafic melts with the low $\varepsilon_{Nd(t)}$ (<0) are inferred to be derived from enriched lithospheric mantle, while the melts with the high $\varepsilon_{Nd(t)}$ (>0) are from the asthenospheric mantle (e.g., Xu 2001). The $\varepsilon_{Nd(t)}$ values of Cenozoic basalts in Chifeng area range from +1.6 to +4.4 (Han et al. 1999), similar to those of Cenozoic basalts in eastern NCC (e.g., Xu 2001; Zhang et al. 2009; Zeng et al. 2010, 2011; Xu et al. 2012), thus favoring an asthenospheric origin. More importantly, geophysical investigations have showed that the present lithosphere thickness beneath Chifeng area is ~100 km (Ma 1987; Chen 2010), in agreement with the inferred melting depth of Xindian basalts (~3.0 GPa; Fig. 10). This is best explained by the lid effect model, in which the final melting depth of asthenosphere-derived basalts is controlled by the thickness of lithosphere above (e.g., Niu et al. 2011).

Pyroxenite in the asthenosphere could be directly transformed from subducted oceanic crust (stage I pyroxenite; e.g., Herzberg 2011), or the reaction product between the subducted oceanic crust and its surrounding depleted peridotite mantle (stage II pyroxenite; e.g., Sobolev et al. 2005; Herzberg 2011). Because MgO contents of some melt inclusions in the Xindian basalts are >8.0 wt%, higher than those of melts yielded by only oceanic crust melting (MgO < 8.0 wt%; e.g., Pertermann and Hirschmann 2004), we prefer the stage II pyroxenite in asthenosphere as the source of the Xindian basalts. Combined with the melting experiments of homogeneous basalt–peridotite mixtures (Kogiso et al. 1998; Yaxley 2000), and no olivine in the residual source of the Xindian basalts, we further infer that the proportion of peridotite involved in the formation of the stage II pyroxenite is less than 50 %.

Since the incompatible trace element concentrations of the surrounding depleted mantle are much lower than those of recycled oceanic crust (e.g., Stracke et al. 2003), their ratios of the stage II pyroxenite with less than 50 % peridotite are nearly similar to those of recycled oceanic crust. We used the average compositions of Zambezi Belt group I and II eclogites reported in John et al. (2004), a good estimate for average recycled oceanic lithosphere (Pfänder et al. 2007), as the compositions of the recycled oceanic crust. We used the moderate incompatible element ratios (Zr/Hf, Lu/Hf and Dy/Yb) to estimate the degrees of pyroxenite melting (Stracke and Bourdon 2009). The proportions of olivine and orthopyroxene in the assumed source are neglected, due to their low mode compositions in the residual source of Xindian basalts and low incompatible element concentrations in these two minerals. Using various clinopyroxene/garnet ratios, we estimate the degrees of partial melting for the Xindian basalts, which are shown in Fig. 11. The results show that the degrees of partial melting are 20–25 % and the clinopyroxene/garnet ratios in the source are probably from 5/1 to 8/1 (Fig. 11). The estimated melting degrees for Xindian basalts are consistent with the degrees of pyroxenite melting experiment at 3.5 GPa (e.g., Sobolev et al. 2007), and the calculated melt fraction from pyroxenite melting at 3.0 GPa within the normal mantle potential temperature (Pertermann and Hirschmann 2003). The mode of garnet in the source is relatively low (<17 %), possibly due to high Al_2O_3 content in clinopyroxene at high pressure (Pertermann and Hirschmann 2003).

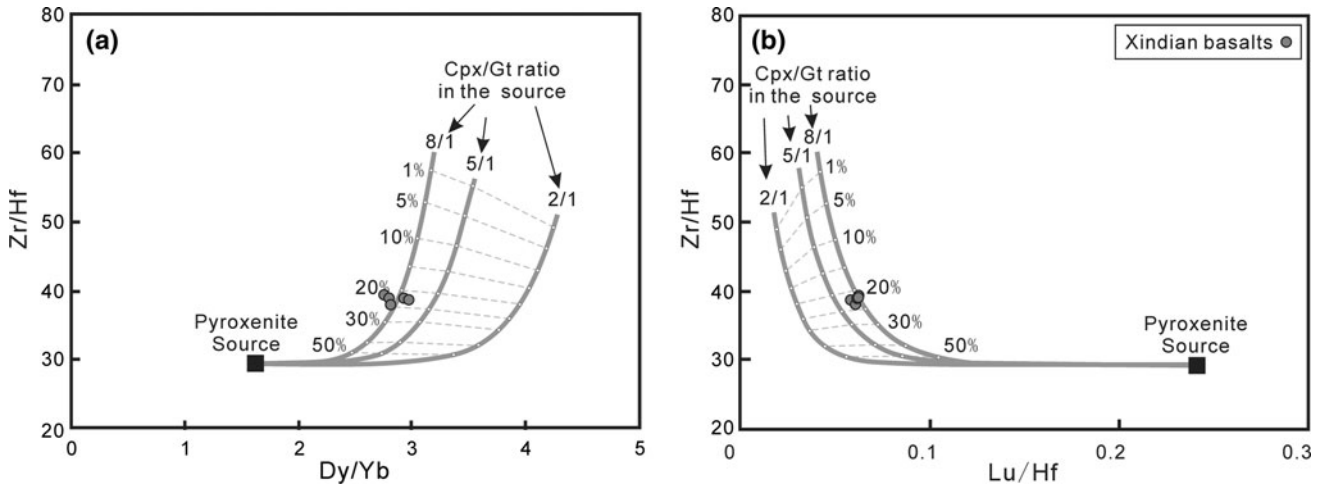

Fig. 11 Fractional melting curves for pyroxenite in terms of Zr/Hf against Dy/Yb (**a**) and Lu/Hf (**b**) for Xindian basalts. The modeled curves are calculated for various clinopyroxene/garnet ratios in the source using partition coefficient data from Pertermann et al. (2004). The compositions of pyroxenite source are from the average compositions of Zambezi Belt group I and II eclogite (John et al. 2004). Melt fraction is displayed as percent along the melting curves

H_2O content in the source of Xindian basalts

Previous studies on peridotite xenoliths in the NCC showed that H_2O contents of these peridotites were generally lower than those of peridotites in other Archaean cratons, and Proterozoic or younger-age off-cratons, and abyssal peridotites (Yang et al. 2008; Xia et al. 2010). This suggests that the Cenozoic lithospheric mantle beneath NCC was rather dry (Yang et al. 2008; Xia et al. 2010). Xia et al. (2010) argued that the dry lithospheric mantle beneath the NCC represents the old lithospheric mantle surviving from the lithospheric destruction, and the low H_2O content was due to the reheating from below by the upwelling asthenospheric flow.

MELTS program is used to simulate the isobaric fractional crystallization process of the Xindian basalts at various pressures and water contents (Ghiorso and Sack 1995; Asimow and Ghiorso 1998; Smith and Asimow 2005). The following parameter ranges are tested: temperature from 1,400 to 1,000 °C, pressure from 500 to 5,000 bar and the starting H_2O content from 0 to 1.0 wt% with the interval of 0.1 wt% for each calculation. The oxygen fugacity of the magma is kept at QFM buffer. A melt inclusion with relatively high MgO (MgO = 8.13 wt%; Fig. 8) content is chosen as the parental magma. In principle, the melt inclusion with the highest MgO is the best candidate for a liquid parental, but in the present case, the inclusion with MgO = 8.51 wt% scatters toward high Al_2O_3 and low SiO_2 compared to the main trend of the data. The inclusion with MgO = 8.13 wt% evolves more closely along the main or average trend of all the inclusion data.

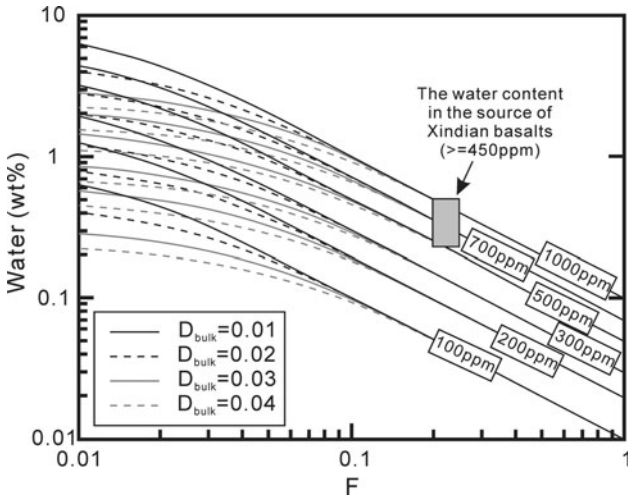

Fig. 12 Fractional melting curves in terms of water content versus melt fraction (F), calculated using various bulk partition coefficient values (D_{bulk}). Since the pyroxenite source of the Xindian basalts may have high pyroxene mode (>50 %), and for pyroxenite, $D_{water}^{pyroxene\text{-}melt}$ is commonly ≥0.02, but <0.04 at pressure of 3.0 GPa (Aubaud et al. 2008), the melting curves of both D_{bulk} <0.01 and D_{bulk} >0.04 are not shown here. The number labeled on the melting curves represents the water content in the source. The water content in the source of Xindian basalts is estimated to be ≥450 ppm

The results of MELTS calculation show that the magma chamber pressure no more than 1,000 bar and H_2O content of 0.3–0.7 wt% at MgO = 8.13 wt% well reproduce the crystallization trend of melt inclusion data of the Xindian basalts (Fig. 8). Pressure higher than 1,000 bar is not suitable, because under that circumstance, calculated SiO_2 contents deviate from the melt inclusion compositions, due to early fractionation of orthopyroxene or clinopyroxene (Fig. 8d). H_2O content in magmas higher than 0.7 wt% and lower than 0.3 wt% is also inappropriate, because higher or lower H_2O content would hamper or accelerate plagioclase fractionation, yielding a magma fractionation trend inconsistent with the observed one (Fig. 8b, c).

Water contents in Xindian basalts may be related to those in the magma source, or to differentiation processes in shallow magma chamber. Recent measurement of H_2O contents of the Xindian melt inclusions shows that H_2O contents decrease with decreasing Fo at Fo > 76 (Hong et al. in prep.). This hints water loss rather than water addition during fractionation. It follows that water content in Xindian basalts reflects that of magma source.

As demonstrated above, the Xindian basalts with MgO > 6.0 wt% were only subjected to olivine fractionation; thus, the composition of primitive melt can be obtained by adding equilibrating olivine into these melts (e.g., Herzberg and Asimow 2008). Assuming that the primitive melt of the Xindian basalts is equilibrated with Fo = 90, MgO content in the primitive melt will be up to 17 wt%, and the water content will be reduced to be 0.23–0.53 wt%. Since there is no evidence for mantle plume in eastern China during Cenozoic (Niu 2005), the MgO content of the primitive melt may be overestimated; as a consequence, 0.23–0.53 wt% represents the minimum estimate of water content in the primitive melts. Using 20–25 % of the melt fraction (Fig. 11), the lowest estimate of water content in the source of Xindian basalts is 450 ppm- >1,000 ppm (Fig. 12), much higher than that in dry lithospheric mantle beneath the NCC (6–85 ppm; Xia et al. 2010). It is necessary to point out that the uncertainty associated with the estimation of water content in the source is relatively large. Direct measurement of water content in melt inclusion is required in future study.

Implications for the lithospheric evolution in eastern NCC

In eastern NCC, the variation of petrochemistry of Cenozoic basalts was related to the temporal change in lithospheric thickness, and tholeiitic basalts from convection mantle were thought to be the signals of the thinnest

lithosphere (DePaolo and Daley 2000; Xu 2001). Thus, change of rock type from tholeiitic basalts in Early Tertiary to alkali and strongly alkali basalts in Late Tertiary and Quaternary was used to infer the lithospheric thickening during Cenozoic (Menzies and Xu 1998; Xu 2001, 2007; Xu et al. 2004).

The above inference as to lithospheric evolution is made under the assumption that all the Cenozoic basalts from eastern China are peridotitic melts. However, this study and other recent investigations (Zhang et al. 2009; Zeng et al. 2011; Xu et al. 2012) show that this is not always the case. Instead, the involvement of pyroxenite in the source is rather common in the genesis of Cenozoic basalts. Caution should therefore be exercised when one estimates the lithospheric thickness using basalt petrochemistry.

The results presented in this study illustrate that the melting pressure of the Xindian tholeiitic basalts possibly reaches ~3.0 GPa (corresponding depth of ~100 km; Fig. 10), much deeper than the melting depth (<60 km) commonly thought for tholeiitic basalts of peridotite source (Fan and Hooper 1991; DePaolo and Daley 2000; Xu 2001). This is consistent with the experimental results which show the lower solidus of pyroxenite than that of peridotite (e.g., Yasuda et al. 1994; Takahashi et al. 1998). If our results are correct in first order, the lithospheric evolution underneath the NCC during Cenozoic should be re-evaluated. We suggest that the occurrence of tholeiitic basalts as an indicator of the thinnest lithosphere can only be applied for the areas with the present thinnest lithosphere, such as around the Bohai basin (~60 km; Ma 1987; Chen 2010), rather than for the whole eastern NCC.

Conclusions

The euhedral and subhedral olivines in the Xindian basalts have CaO contents higher than 0.15 wt% and contain melt inclusions, indicating that they are phenocrysts crystallizing from magma. The crystallization sequence is inferred as follows: olivine → plagioclase → clinopyroxene → ilmenite. The melt inclusions from the Xindian basalts are tholeiitic in compositions and have low Ca and Mn contents, and high Ni contents and Fe/Mn ratios. Melt inclusions with high MgO (>6.0 wt%) have low CaO contents. In CS-MS-A diagram, the residual minerals in their source are mainly clinopyroxene and garnet, possibly subordinate orthopyroxene, but no olivine. All these suggest that the Xindian basalts were derived from a pyroxenite source rather than a peridotite source. Modeling calculations using MELTS program show that H_2O content in the Xindian basalts is 0.3–0.7 wt% at MgO = 8.13 wt%. Using melt fraction of 20–25 %, the H_2O content in the source is estimated to be ≥450 ppm, much higher than that in the lithospheric mantle (6–85 ppm). The melting depth of Xindian tholeiitic basalts might have reached ~100 km, considerably deeper than the conventionally thought for tholeiitic basalts (<60 km). This is consistent with the lower solidus of pyroxenite, compared to that of peridotite. Therefore, it is necessary to define first the source lithology of basalts before using their compositions to constrain the lithospheric evolution.

Acknowledgments We thank Y Liu, LL Chen and L Wu for technical assistance with XRF and EPMA analyses. We also thank XL Tu and GQ Hu for the ICP-MS analyses. Thoughtful and thorough reviews by Paul D. Asimow and an anonymous reviewer are greatly appreciated. Their suggestions greatly improve this paper. Financial supports from the National Natural Science Foundation of China (90714001; 91014007), the "hundred talent project" of Chinese Academy of Sciences and the CAS/SAFEA International Partnership Program for Creative Research Teams (KZCX2-YW-Q04-06) are gratefully acknowledged. This is GIGCAS Publication No.1554.

References

Asimow PD, Ghiorso MS (1998) Algorithmic modifications extending MELTS to calculate subsolidus phase relations. Am Mineral 83:1127–1132

Asimow PD, Langmuir CH (2003) The importance of water to oceanic mantle melting regimes. Nature 421:815–820

Asimow PD, Dixon JE, Langmuir CH (2004) A hydrous melting and fractionation model for mid-ocean ridge basalts: application to the Mid-Atlantic Ridge near the Azores. Geochem Geophys Geosyst 5. doi:10.1029/2003GC000568

Aubaud C, Hirschmann MM, Withers AC, Hervig R (2008) Hydrogen partition between melt, clinopyroxene, and garnet at 3 GPa in a hydrous MORB with 6 wt% H_2O. Contrib Mineral Petrol 156:607–625

Balta JB, Asimow PD, Mosenfelder JL (2011) Manganese partitioning during hydrous melting of peridotite. Geochim Cosmochim Acta 75:5819–5833

Beattie P, Ford C, Russell D (1991) Partition coefficients for olivine-melt and orthopyroxene-melt systems. Contrib Mineral Petrol 109:212–224

Blundy J, Cashman K (2008) Petrologic reconstruction of magmatic system variables and processes. Rev Mineral Geochem 69:179–239

Chen L (2010) Concordant structural variations from the surface to the base of the upper mantle in the North China Craton and its tectonic implications. Lithos 120:96–115

Chen LH, Zeng G, Jiang SY, Hofmann AW, Xu XS (2009) Sources of Anfengshan basalts: subducted lower crust in the Sulu UHP belt, China. Earth Planet Sci Lett 286:426–435

Chu ZY, Wu FY, Walker RJ, Rudnick RL, Pitcher L, Puchtel IS, Yang YH, Wilde SA (2009) Temporal evolution of the lithospheric mantle beneath the Eastern NCC. J Petrol 50:1857–1898

Danyushevsky LV, Della-Pasqua FN, Sokolov S (2000) Re-equilibration of melt inclusions trapped by magnesian olivine phenocrysts from subduction-related magmas: petrological implications. Contrib Mineral Petrol 138:68–83

Danyushevsky LV, McNeill AW, Sobolev AV (2002) Experimental and petrological studies of melt inclusions in phenocrysts from mantle-derived magmas: an overview of techniques, advantages and complications. Chem Geol 183:5–24

DePaolo DJ, Daley EE (2000) Neodymium isotopes in basalts of the southwest basin and range and lithospheric thinning during continental extension. Chem Geol 169:157–185

Falloon TJ, Danyushevsky LV (2000) Melting of refractory mantle at 1.5, 2 and 2.5 GPa under anhydrous and H_2O-undersaturated conditions: implications for the petrogenesis of high-Ca boninites and the influence of subduction components on mantle melting. J Petrol 41:257–283

Fan QC, Hooper PR (1989) The mineral chemistry of ultramafic xenoliths of Eastern China: implications for upper mantle composition and the paleogeotherms. J Petrol 30:1117–1158

Fan QC, Hooper PR (1991) The Cenozoic basaltic rocks of Eastern China: petrology and chemical composition. J Petrol 32:765–810

Fan WM, Zhang HF, Baker J, Jarvis KE, Mason PRD, Menzies MA (2000) On and off the NCC: where is the Archaean keel? J Petrol 41:933–950

Ford CE, Russell DG, Craven JA, Fisk MR (1983) Olivine-liquid equilibria: temperature, pressure, and composition dependence of the crystal/liquid cation partition coefficient for Mg, Fe^{2+}, Ca and Mn. J Petrol 24:256–266

Frezzotti ML (2001) Silicate-melt inclusions in magmatic rocks: applications to petrology. Lithos 55:273–299

Gaetani GA, Grove TL (1998) The influence of water on melting of mantle peridotite. Contrib Mineral Petrol 131:323–346

Gao S, Rudnick RL, Carlson RW, McDonough WF, Liu YS (2002) Re-Os evidence for replacement of ancient mantle lithosphere beneath the North China Craton. Earth Planet Sci Lett 198: 307–322

Gao S, Rudnick RL, Yuan HL, Liu XM, Liu YS, Xu WL, Ling WL, Ayers J, Wang XC, Wang QH (2004) Recycling lower continental crust in the North China craton. Nature 432:892–897

Gao S, Rudnick RL, Xu WL, Yuan HL, Liu YS, Walker RJ, Puchtel IS, Liu XM, Huang H, Wang XR, Yang J (2008) Recycling deep cratonic lithosphere and generation of intraplate magmatism in the North China Craton. Earth Planet Sci Lett 270:41–53

Garcia MO, Hulawvoaxh RP, Ehoswa JM (1995) Olivine-rich submarine basalts from the southwest rift zone of Mauna Loa Volcano: Implications for magmatic processes and geochemical evolution. In: Rhodes JM and Lockwood JP (eds) Mauna Loa Decade Volcano. Am Geophys Union, Geophys Monogr 92: 219–239

Ghiorso MS, Sack RO (1995) Chemical mass transfer in magmatic processes. IV. A revised and internally consistent thermodynamic model for the interpolation and extrapolation of liquid-solid equilibria in magmatic systems at elevated temperatures and pressures. Contrib Mineral Petrol 119:197–212

Goto A, Tatsumi Y (1996) Quantitative analyses of rock samples by an X-ray fluorescence spectrometer (II). Rigaku J 13:20–39

Green DH, Ringwood AE (1963) Mineral assemblages in a model mantle composition. J Geophys Res 68:937–945

Griffin WL, Zhang AD, O'Reilly SY, Ryan G (1998) Phanerozoic evolution of the lithosphere beneath the Sino-Korean Craton. In: Flower M, Chung SL, Lo CH, Lee TY (eds) Mantle dynamics and plate interaction in east Asia. AGU Geodynamic Series 27:107–126

Gurenko AA, Chaussidon M (1995) Enriched and depleted primitive melts included in olivine from Icelandic tholeiites: origin by continuous melting of a single mantle column. Geochim Cosmochim Acta 59:2905–2917

Han BF, Wang SG, Kagami H (1999) Trace element and Nd-Sr isotope constraints on origin of the Chifeng flood basalts, North China. Chem Geol 155:187–199

Hart SR, Davis KE (1978) Nickel partitioning between olivine and silicate melt. Earth Planet Sci Lett 40:203–219

Hauri EH (1996) Major element variability in the Hawaiian mantle plume. Nature 382:415–419

Hauri EH, Hart SR (1993) Re-Os isotope systematics of HIMU and EMI oceanic island basalt from the South Pacific Ocean. Earth Planet Sci Lett 114:353–371

Herzberg C (2006) Petrology and thermal structure of the Hawaiian plume from Mauna Kea volcano. Nature 444:605–609

Herzberg C (2011) Identification of source lithology in the Hawaiian and Canary Islands: implications for origin. J Petrol 52:113–146

Herzberg C, Asimow PD (2008) Petrology of some oceanic island basalts: PRIMELT2.XLS software for primary magma calculation. Geochem Geophys Geosyst 9. doi:10.1029/2008GC002057

Hirschmann MM, Stolper EM (1996) A possible role for garnet pyroxenite in the origin of the 'garnet signature' in MORB. Contrib Mineral Petrol 124:185–208

Hofmann AW (1997) Mantle geochemistry: the message from oceanic volcanism. Nature 385:219–229

Hofmann AW, White WM (1982) Mantle plumes from ancient oceanic crust. Earth Planet Sci Lett 57:421–436

Jackson MG, Hart SR (2006) Strontium isotopes in melt inclusions from Samoan basalts: implications for heterogeneity in the Samoan plume. Earth Planet Sci Lett 245:260–277

Jahn BM, Auvray B, Cornichet J, Bai YL, Shen QH, Liu DY (1987) 3.5 Ga old amphibolites from eastern Hebei province China: field occurrence, petrography, Sm-Nd isochron age and REE geochemistry. Precam Res 34:311–346

Jia W, Zhu HZ, Shao JA (2002) Temporal-spatial distribution of Cenozoic basalts in Chifeng area. Inner Mongolia. Geol Rev 48:267–272 (in Chinese with English abstract)

John T, Scherer EE, Haase K, Schenk V (2004) Trace element fractionation during fluid-induced eclogitization in a subducting slab: trace element and Lu-Hf-Sm-Nd isotope systematics. Earth Planet Sci Lett 227:441–456

Kamenetsky VS (2006) Melt inclusion record of magma immiscibility in crustal and mantle magmas. In: Melt inclusions in plutonic rocks. MAC, Short Course Series 36:81–98

Kamenetsky VS, Gurenko AA (2007) Cryptic crustal contamination of MORB primitive melts recorded in olivine-hosted glass and mineral inclusions. Contrib Mineral Petrol 153:465–481

Kamenetsky VS, Elurg M, Arculus R, Thomas R (2006) Magmatic origin of low-Ca olivine in subduction-related magmas: co-existence of contrasting magmas. Chem Geol 233:346–357

Kent AJR (2008) Melt inclusions in basaltic and related volcanic rocks. Rev Mineral Geochem 69:273–331

Kent AJR, Clague DA, Honda M, Stolper EM, Hutcheon ID, Norman MD (1999) Widespread assimilation of a seawater-derived component at Loihi Seamount, Hawaii. Geochim Cosmochim Acta 63:2749–2761

Kent AJR, Baker JA, Wiedenbeck M (2002) Contamination and melt aggregation processes in continental flood basalts: constraints from melt inclusions in Oligocene basalts from Yemen. Earth Planet Sci Lett 202:577–594

Kinzler RJ, Grove TL (1992a) Primary magmas of mid-ocean ridge basalts 1. experiments and methods. J Geophys Res 97: 6907–6926

Kinzler RJ, Grove TL (1992b) Primary magmas of mid-ocean ridge basalts 2. Applications. J Geophys Res 97:6907–6926

Kinzler RJ, Grove TL, Recca SI (1990) An experimental study on the effect of temperature and melt composition on the partitioning of nickel between olivine and silicate melt. Geochim Cosmochim Acta 54:1255–1265

Kogiso T, Hirose K, Takahashi E (1998) Melting experiments on homogeneous mixtures of peridotite and basalt: application to the genesis of ocean island basalts. Earth Planet Sci Lett 162: 45–61

Kogiso T, Hirschmann MM, Pertermann M (2004) High-pressure partial melting of mafic lithologies in the mantle. J Petrol 45: 2407–2422

Kovalenko VI, Naumov VB, Yarmolyuk VV, Dorofeeva VA (2000) Volatile components (H_2O, CO_2, Cl, F and S) in basic magmas of various geodynamic settings: data on melt inclusions and quenched glasses. Petrology 8:113–144

Kushiro I (1968) Compositions of magmas formed by partial melting of the Earth's upper mantle. J Geophys Res 73:619–634

Kushiro I (1969) The system forsterite-diopside-silica with and without water at high pressures. Am J Sci 267A:269–294

Kushiro I (1972) Effect of water on the composition of magmas formed at high pressures. J Petrol 13:311–334

Lassiter JC, Hauri EH (1998) Osmium-isotope variations in Hawaiian lavas: evidence for recycled oceanic lithosphere in Hawaiian Plume. Earth Planet Sci Lett 164:483–496

Le Bas MJ, Le Maitre RW, Streckeisen A, Zanettin B (1986) A chemical classification of volcanic rocks based on the total alkali-silica diagram. J Petrol 27:745–750

Liu CQ, Masuda A, Xie GH (1992a) Major element compositions and rare-earth element abundances of Cenozoic basalts in Eastern China: implications for a pressure control over LREE/HREE fractionation in continental basalts. Chin J Geochem 11:289–313

Liu DY, Nutman AP, Compston W, Wu JS, Shen QH (1992b) Remnants of 3800 Ma crust in Chinese part of the Sino-Korean craton. Geology 20:339–342

Liu RX, Chen WJ, Sun JZ, Li DM (1992c) The K-Ar age and tectonic environment of Cenozoic volcanic rock in China. In: Liu RX (ed) The age and geochemistry of Cenozoic volcanic in China. Seismological Press, Beijing, pp 1–43 (in Chinese)

Liu Y, Liu HC, Li XH (1996) Simultaneous and precise determination of 40 trace elements in rock samples by ICP-MS. Geochim 25:552–558 (in Chinese with English abstract)

Liu X, O'Neill HSC, Berry AJ (2006) The effects of small amounts of H_2O, CO_2, and Na_2O on the partial melting of spinel lherzolite in system CaO-MgO-Al_2O_3-SiO_2 ± H_2O ± CO_2 ± Na_2O at 1.1 GPa. J Petrol 47:409–434

Longhi J (2002) Some phase equilibrium systematics of lherzolite melting: I. Geochem Geophys Geosyst 3. doi:10.1029/2001GC000204

Lowenstern JB (1995) Applications of silicate-melt inclusions to the study of magmatic volatiles. In: Thompson JFH (ed) Magmas, fluids, and ore deposits. MAC short course series 23:71–99

Lowenstern JB (2003) Melt inclusions come of age: volatiles, volcanoes, and Sorby's legacy. In: Vivo BD, Rodnar RJ (eds) Melt inclusions in volcanic system: methods, applications and problems. Developments in volcanology, vol 5. Elsevier, Amsterdam, pp 1–22

Luo XQ, Chen QT (1990) Preliminary study on geochronology for Cenozoic basalts from Inner Mongolia. Acta Petrol Mineral 9:37–46 (in Chinese with English abstract)

Lustrino M (2005) How the delamination and detachment of lower crust can influence basaltic magmatism. Earth-Sci Rev 72:21–38

Ma XY (1987) Lithospheric dynamics map of China and adjacent seas (1:4,000,000) and explanatory notes. Geological Publishing House, Beijing (in Chinese)

McDonough WF, Ireland TR (1993) Intraplate origin of Komatiites inferred from trace elements n glass inclusions. Nature 365: 432–434

McDonough WF, Sun S–S (1995) The composition of the Earth. Chem Geol 120:223–253

McKenzie D, Bickle MJ (1988) The volume and composition of melt generated by extension of the lithosphere. J Petrol 29:625–679

McKenzie D, O'Nions K (1991) Partial melt distributions from inversion of rare earth element concentrations. J Petrol 32:1021–1091

Menzies MA, Xu YG (1998) Geodynamics of the North China Craton. In: Flower M, Chung SL, Lo CH, Lee TY (eds) Mantle dynamics and plate interactions in east Asia. AGU Geodynamic Series 27:155–165

Menzies MA, Fan WM, Zhang M (1993) Palaeozoic and Cenozoic lithoprobes and the loss of > 120 km of Archaean lithosphere, Sino-Korean craton, China. In: Prichard HM, Alabaster T, Harris NBW, Neary CR (eds) Magmatic processes and plate tectonics. Geol Soc Spe Publ 76:71–78

Menzies MA, Xu YG, Zhang HF, Fan WM (2007) Integration of geology, geophysics and geochemistry: a key to understanding the North China Craton. Lithos 96:1–21

Métrich N, Wallace PJ (2008) Volatile abundances in basaltic magmas and their degassing paths tracked by melt inclusions. Rev Mineral Geochem 69:363–402

Moore G (2008) Interpreting H_2O and CO_2 contents in melt inclusions: constraints from solubility experiments and modeling. Rev Mineral Geochem 69:333–361

Mysen BO, Virgo D, Harrison WJ, Scarfe CM (1980) Solubility mechanisms of H_2O in silicate melts at high pressures and temperatures: a Raman spectroscopic study. Am Mineral 65: 900–914

Nielsen RL, Crum J, Bourgeois R, Hascall K, Forsythe LM, Fisk MR, Christie DM (1995) Melt inclusions in high-An plagioclase from the Gorda Ridge: an example of the local diversity of MORB parent magmas. Contrib Mineral Petrol 122:34–50

Niu YL (2005) Generation and evolution of basaltic magmas: some basic concepts and a new view on the origin of Mesozoic-Cenozoic basaltic volcanism in eastern China. Geol J Chin Univ 11:9–46

Niu YL, O'Hara MJ (2007) Varying Ni in OIB olivines-product of process not source. Geochim Cosmochim Acta 71:A721

Niu YL, Wilson M, Humphreys ER, O'Hara MJ (2011) The origin of intra-plate ocean island basalts (OIB): the lid effect and its geodynamic implications. J Petrol 52:1443–1468

Norman MN, Garcia MO, Kamenetsky VS, Nielsen RL (2002) Olivine-hosted melt inclusions in Hawaiian picrites: equilibration, melting and plume source characteristics. Chem Geol 183: 143–168

Parman SW, Grove TL (2004) Harzburgite melting with and without H_2O: experiment data and predictive modeling. J Geophys Res 109:B02201

Pertermann M, Hirschmann MM (2003) Anhydrous partial melting experiments on MORB-like eclogite: phase relations, phase compositions and mineral-melt partitioning of major element at 2–3 GPa. J Petrol 44:2173–2201

Pertermann M, Hirschmann MM (2004) Anhydrous partial melting experiments on MORB-like eclogite: phase relations, phase compositions and mineral-melt partitioning of major elements at 2–3 GPa. J Petrol 44:2173–2201

Pertermann M, Hirschmann MM, Hametner K, Günther D, Schmidt MW (2004) Experimental determination of trace element partitioning between garnet and silica-rich liquid during anhydrous partial melting of MORB-like eclogite. Geochem Geophys Geosyst 5. doi:10.1029/2003GC000638

Pfänder JA, Münker C, Stracke A, Mezger K (2007) Nb/Ta and Zr/Hf in oceanic island basalts-implications for crust-mantle differentiation and the fate of Niobium. Earth Planet Sci Lett 254: 158–172

Portnyagin M, Hoernle K, Plechov P, Mironov N, Khubunaya S (2007) Constraints on mantle melting and composition and nature of slab components in volcanic arcs from volatiles (H_2O, S, Cl, F) and trace elements in melt inclusions from the Kamchatka Arc. Earth Planet Sci Lett 255:53–69

Putirka KD (2005) Mantle potential temperatures at Hawaii, Iceland, and the mid-ocean ridge system, as inferred from olivine phenocrysts: Evidence for thermally driven mantle plumes. Geochem Geophys Geosyst 6. doi:10.1029/2005GC000915

Putirka KD, Ryerson FJ, Perfit M, Ridley WI (2011) Mineralogy and composition of the Oceanic Mantle. J Petrol 52:279–313

Ren ZY, Takahashi E, Orihashi Y, Johnson KTM (2004) Petrogenesis of tholeiitic lavas from the submarine Hana Ridge, Haleakala Volcano, Hawaii. J Petrol 45:2067–2099

Ren ZY, Ingle S, Takahashi E, Hirano N, Hirata T (2005) The chemical structure of the Hawaiian mantle plume. Nature 436:837–840

Ren ZY, Shibata T, Yoshikawa M, Johnson K, Takahashi E (2006) Isotope compositions of submarine Hana ridge lavas, Haleakala volcano, Hawaii. J Petrol 45:2067–2099

Ren ZY, Hanyu T, Miyazaki T, Chang Q, Kawabata H, Takahashi T, Hirahara Y, Nichols ARL, Tatsumi Y (2009) Geochemical differences of the Hawaiian shield lavas: implications for melting process in the heterogeneous Hawaiian plume. J Petrol 50:1553–1573

Rhodes JM, Huang SC, Frey FA, Pringle M, Xu GP (2012) Compositional diversity of Mauna Kea shield lavas recovered by the Hawaii Scientific Drilling Project: inferences on source lithology, magma supply, and the role of multiple volcanoes. Geochem Geophys Geosyst 13. doi: 10.1029/2011GC003812

Ringwood AE (1975) Composition and petrology of the earth's mantle. McGraw-Hill, New York, p 618

Roedder E (1979) Origin and significance of magmatic inclusions. Bull Mineral 102:487–501

Rudnick RL, Gao S, Ling WL, Liu YS, McDonough WF (2004) Petrology and geochemistry of spinel peridotite xenoliths from Hannuoba and Qixia, NCC. Lithos 77:609–637

Saal AE, Hart SR, Shimizu N, Hauri EH, Layne GD (1998) Pb isotopic variability in melt inclusions from oceanic island basalts, Polynesia. Science 282:481–484

Saal AE, Hart SR, Shimizu N, Hauri EH, Layne GD, Eiler JM (2005) Pb isotopic variability in melt inclusions from the EMI-EMII-HIMU mantle end-members and the role of the oceanic lithosphere. Earth Planet Sci Lett 240:605–620

Schiano P (2003) Primitive mantle magmas recorded as silicate melt inclusions in igneous minerals. Earth Sci Rev 63:121–144

Shi RP, Zhu RX, Pan YX, Shi GH (2002) Paleointensity study of Early Miocene lavas from Pingzhuang, Inner Mongolia, China. Geophys Res Lett 29(21). doi:10.1029/2002GL015990

Shi RP, Hill MJ, Zhu RX, He HY, Shaw J (2005) $^{40}Ar/^{39}Ar$ dating and preliminary paleointensity determination on a single lava flow from Chifeng, Inner Mongolia. Phys Earth Planet In 152:78–89

Simkin T, Smith JV (1970) Minor-element distribution in olivine. J Geol 78:304–325

Smith PM, Asimow PD (2005) Adiabat_1ph: a new public front-end to the MELTS, pMELTS, and pHMELTS models. Geochem Geophys Geosyst 6. doi:10.1029/2004GC000816

Sobolev AV (1996) Melt inclusions in minerals as a source of principle petrological information. Petrology 4:209–220

Sobolev AV, Chaussidon M (1996) H_2O concentrations in primary melts from suprasubduction zones and mid-ocean ridges: implications for H_2O storage and recycling in the mantle. Earth Planet Sci Lett 137:45–55

Sobolev VS, Kostyuk VP (1975) Magmatic crystallization based on a study of melt inclusions. Fluid Incl Res 9:182–235

Sobolev AV, Shimizu N (1993) Ultra-depleted primary melt included in an olivine from the Mid-Atlantic ridge. Nature 363:151–154

Sobolev AV, Hofmann AW, Sobolev SV, Nikogosian IK (2005) An olivine-free mantle source of Hawaiian shield basalts. Nature 434:590–597

Sobolev AV, Hofmann AW, Kuzmin DV et al (2007) The amount of recycled crust in sources of mantle-derived melts. Science 316:412–417

Song B, Nutman AP, Liu DY, Wu JS (1996) 3800 to 3500 Ma crustal evolution in Anshan area of Liaoning Province, Northeastern China. Precam Res 78:79–94

Sorby HC (1858) On the microscopic structures of crystals, indicating the origin of minerals and rocks. Geol Soc Q J 14:453–500

Sours-Page RL, Johnson KTM, Batiza R (2002) Melt inclusions as indicators of parental magma diversity on the northern East Pacific Rise. Chem Geol 183:237–261

Stracke A, Bourdon B (2009) The importance of melt extraction for tracing mantle heterogeneity. Geochim Cosmochim Acta 73: 218–238

Stracke A, Bizimis M, Salters VJM (2003) Recycling oceanic crust: quantitative constraints. Geochem Geophys Geosyst 4. doi: 10.1029/2001GC000223

Stracke A, Hofmann AW, Hart SR (2005) FOZO, HIMU and the rest of the mantle zoo. Geochem Geophys Geosyst 6. doi:10.1029/2004GC000824

Takahashi E, Nakajima K, Wright TL (1998) Origin of the Columbia River basalts: melting model of a heterogeneous plume head. Earth Planet Sci Lett 162:63–80

Wagner TP, Grove TL (1998) Melt/harzburgite reaction in the petrogenesis of tholeiitic magma from Kilauea volcano, Hawaii. Contrib Mineral Petrol 131:1–12

Walker JA, Roggensack K, Patino LC, Cameron BI, Matias O (2003) The water and trace element contents of melt inclusions across an active subduction zone. Contrib Mineral Petrol 146:62–77

Walter MJ (1998) Melting of garnet peridotite and the origin of komatiite and depleted lithosphere. J Petrol 39:29–60

Wang ZR, Gaetani GA (2008) Partitioning of Ni between olivine and siliceous eclogite partial melt: experimental constraints on the mantle source of Hawaiian basalts. Contrib Mineral Petrol 156:661–678

Wang Y, Zhao ZF, Zheng YF, Zhang JJ (2011) Geochemical constraints on the nature of mantle source for Cenozoic continental basalts in east-central China. Lithos 125:940–955

Weaver BL (1991) Trace element evidence for the origin of ocean-island basalts. Geology 19:123–126

Willbold M, Stracke A (2006) Trace element composition of mantle end-members: implications for recycling of oceanic and upper and lower continental crust. Geochem Geophys Geosyst 7. doi: 10.1029/2005GC001005

Wood BJ, Turner SP (2009) Origin of primitive high-Mg andesite: constraints from natural examples and experiments. Earth Planet Sci Lett 283:59–66

Wu FY, Sun DY, Zhang GL, Ren XW (2000) Deep geodynamics of Yanshain movement. Geol J Chin Univ 6:379–388 (in Chinese with English abstract)

Wu FY, Walker RJ, Ren XW, Sun DY, Zhou XH (2003) Osmium isotopic constrains on the age of lithospheric mantle beneath northeastern China. Chem Geol 196:107–129

Wu FY, Lin JQ, Wilde SA, Zhang XO, Yang JH (2005a) Nature and significance of the Early Cretaceous giant igneous event in Eastern China. Earth Planet Sci Lett 233:103–119

Wu FY, Yang JH, Wilde SA, Zhang XO (2005b) Geochronology, petrogenesis and tectonic implications of Jurassic granites in the Liaodong Peninsula, NE China. Chem Geol 221:127–156

Wu FY, Zhao GC, Wilde SA, Sun DY (2005c) Nd isotopic constrains on the crustal formation in the NCC. J Asian Earth Sci 24:523–545

Xia QK, Hao YT, Li P, Deloule E, Coltorti M, Dallai L, Yang XZ, Feng M (2010) Low water content of the Cenozoic lithospheric mantle beneath the eastern part of the NCC. J Geophys Res. doi: 10.1029/2009JB006694

Xiao Y, Zhang HF, Fan WM, Ying JF, Zhang J, Zhao XM, Su BX (2010) Evolution of lithospheric mantle beneath the Tan-Lu zone, eastern NCC: evidence from petrology and geochemistry of peridotite xenoliths. Lithos 117:229–246

Xu YG (2001) Thermo-tectonic destruction of the Archaean lithospheric keel beneath eastern China: evidence, timing and mechanism. Phys Chem Earth A 26:747–757

Xu YG (2007) Diachronous lithospheric thinning of the North China Craton and formation of the Daxin'anling-Taihangshan gravity lineament. Lithos 96:281–298

Xu YG, Bodinier JL (2004) Contrasting enrichments in high- and low-Temperature mantle xenoliths from Nushan, Eastern China: results of a single metasomatic event during lithospheric accretion. J Petrol 45:321–341

Xu YG, Chung SL, Ma JL, Shi LB (2004) Contrasting Cenozoic lithospheric evolution and architecture in the western and eastern Sino-Korean Craton: constraints from geochemistry of basalts and mantle xenoliths. J Geol 112:593–605

Xu YG, Li HY, Pang CJ, He B (2009) On the timing and duration of the destruction of the North China Craton. Chin Sci Bull 54:1974–1989 (in Chinese with English abstract)

Xu YG, Zhang HH, Qiu HN, Ge WC, Wu FY (2012) Oceanic crust components in continental basalts from Shuangliao, Northeast China: derived from the mantle transition zone? Chem Geol. doi: 10.1016/j.chemgeo.2012.01.027

Yang XZ, Xia QK, Deloule E, Dallai K, Fan QC, Feng M (2008) Water in minerals of the continental lithospheric mantle and overlying lower crust: a comparative study of peridotite and granulite xenoliths from the NCC. Chem Geol 256:33–45

Yasuda A, Fujii T, Kurita K (1994) Melting phase relations of an anhydrous mid-ocean ridge basalt from 3–20 GPa: implications for the behavior of subducted oceanic crust in the mantle. J Geophys Res 99:9401–9414

Yaxley GM (2000) Experimental study of the phase and melting relations of homogeneous basalt + peridotite mixtures and implications for the petrogenesis of flood basalts. Contrib Mineral Petrol 139:326–338

Zeng G, Chen LH, Xu XS, Jiang SY, Hofmann AW (2010) Carbonated mantle sources for Cenozoic intra-plate alkaline basalts in Shandong, North China. Chem Geol 273:35–45

Zeng G, Chen LH, Hofmann AW, Jiang SY, Xu XS (2011) Crust recycling in the source of two parallel volcanic chains in Shandong, North China. Earth Planet Sci Lett 302:359–368

Zhang HF, Sun M, Zhou XH, Zou MF, Fan WM, Zheng JP (2003) Secular evolution of the lithosphere beneath the eastern NCC: evidence from Mesozoic basalts and high-Mg andesites. Geochim Cosmochim Acta 67:4373–4387

Zhang JJ, Zheng YF, Zhao ZF (2009) Geochemical evidence for interaction between oceanic crust and lithospheric mantle in the origin of Cenozoic continental basalts in east-central China. Lithos 110:305–326

Zhao XX, Riisager P, Riisager J, Draeger U, Coe RS, Zheng Z (2004) New palaeointensity results from Cretaceous basalt of Inner Mongolia, China. Phys Earth Planet In 141:131–140

Zheng JP, O'Reilly SY, Griffin WL, Lu FX, Zhang M (1998) Nature and evolution of Cenozoic lithospheric mantle beneath Shandong Peninsula North China Platform. Int Geol Rev 40: 471–499

Zheng JP, O'Reilly SY, Griffin WL, Lu FX, Zhang M, Pearson NJ (2001) Relict refractory mantle beneath the eastern North China block: significance for lithosphere evolution. Lithos 57:43–66

Zheng Z, Tanaka H, Tatsumi Y, Kono M (2002) Basalt platforms in Inner Mongolia and Hebei Province, northeastern China: new K-Ar ages, geochemistries, and revision of palaeomagnetic results. Geophys J Int 151:654–662

Zheng JP, Griffin WL, O'Reilly SY, Lu FX, Wang CY, Zhang M, Wang FZ, Li HM (2004) 3.6 Ga lower crust in central China: new evidence on the assembly of the NCC. Geology 32: 229–232

Zheng JP, Griffin WL, O'Reilly SY, Li TF, Zhang M, Zhang RY, Liou JG (2006) Mineral chemistry of peridotites from Paleozoic, Mesozoic and Cenozoic lithosphere: constraints on mantle evolution beneath eastern China. J Petrol 47:2233–2256